Article Title: Distinct TCR repertoire diversity, distribution, clonality gene segment use and MHC-restriction in foetal and young adult thymus

Running Title: Foetal αβ TCR repertoire

Authors: Jasmine Rowell[1], Ching-In Lau[1], Susan Ross[1], Diana C. Yanez[1], Benny Chain[2] and Tessa Crompton[1⌘]

Affiliations of authors:

[1]UCL Great Ormond Street Institute of Child Health

30 Guilford Street

London WC1N 1EH, UK

[2] Division of Infection and Immunity

University College London

London, United Kingdom

⌘Address correspondence to Tessa Crompton, Phone: +44 (0)207 905 2893; Fax: +44 (0)207 813 8494; email: t.crompton@ucl.ac.uk

Key words: T-cell development, embryo, T cell receptor (TCR), Positive selection, TCR sequencing, TCR repertoire

Abstract

Here we sequenced rearranged TCRβ and TCRα chain sequences in CD4+CD8+ double positive (DP), CD4+CD8- single positive (SP4) and CD4-CD8+ (SP8) thymocyte populations from the foetus and young adult mouse. This showed that the TCRβ repertoire was less diverse and less evenly distributed in foetus compared to young adult. The predicted TCRβ CDR3 length and number of non-template insertions were lower than adult in each foetal population, but this difference alone did not account for the reduction in diversity, as all foetal populations contained more clonotypic expansions than adult. We found that life-stage had a greater impact on TCRβ and TCRα gene segment usage than cell-type. Foetal repertoires showed bias towards 3'TRAV and 5'TRAJ rearrangements in all populations, whereas adult repertoires used more 5'TRAV gene segments, suggesting that progressive TCRα rearrangements occur less frequently in foetal DP cells. When we synchronised young adult DP thymocyte differentiation by hydrocortisone treatment the new recovering DP thymocyte population showed more foetal-like 3'TRAV and 5'TRAJ gene segment usage. In foetus we identified less influence of MHC-restriction on β-chain combinatorial VxJ usage and predicted α and β CDR1xCDR2 usage in SP compared to adult, indicating weaker impact of MHC-restriction on the foetal TCR repertoire.

Introduction

The thymus is essential for T-cell development and TCR repertoire selection, but undergoes changes in output and function across the life of a mouse(Kondo et al., 2019, Montecino-Rodriguez and Dorshkind, 2023). In this study, we compared the αβTCR repertoire generated in the foetal thymus to that of the young adult, to investigate how these life-stages influence V(D)J gene usage and TCR repertoire diversity and distribution.

A diverse pool of αβTCR is essential for adaptive immunity and is generated during T-cell development in the thymus by the RAG-dependent joining of variable (V), joining (J), and diversity (D) gene segments at the β locus, and V and J gene segments at the α locus, with additional diversity coming from non-template nucleotides (junctional diversity)(Schatz and Swanson, 2011).

The thymus and the parathyroid organs, emerge from the third pharyngeal pouch and cleft during mid gestation of the foetal mouse(Gordon and Manley, 2011). Haematopoietic progenitors migrate from the foetal liver through the blood stream to colonise the thymus from embryonic day (E) 10-12. The first CD4-CD8- double negative (DN) thymocytes are already present at E11 and proliferate over the following days, producing a larger population by E14. CD4+CD8+ double positive (DP) and CD8+ immature single positive (ISP) thymocytes are first detectable at ~E16, while mature CD4+CD8-CD3+ single positive (SP4) and CD4-CD8+CD3+ single positive (SP8) thymocytes can be detected at day E18(Solanki et al., 2018, Solanki et al., 2020). After birth, the thymus continues to grow rapidly and reaches its peak size at 4 to 6 weeks of age(Xiao et al., 2003).

During this developmental progression, the *T cell receptor (TCR)β* and *TCRα* loci are sequentially rearranged to produce T-cells with a diverse TCR repertoire. Successful rearrangement of *TCRβ* and pre-TCR expression are required for commitment to the αβT-cell lineage and differentiation from the CD25+DN (DN3) stage to DP cell, whereas cells that successfully rearrange the γδTCR commit to the γδT-cell lineage at the CD25+DN stage. *TCRα*

rearrangement and signalling through the αβTCR are essential for MHC-restriction and differentiation from DP to SP cell (positive selection) and then also for deletion of T-cells bearing self-reactive TCR (negative selection). Pre-TCR signalling is required for survival, expansion and differentiation of cells that have completed TCRβ rearrangement, to produce a pool of cells which express a single functional TCRβ chain, in which TCRα rearrangement and αβTCR repertoire selection will occur(Dutta et al., 2021). In general, allelic exclusion of the TCRβ chain locus is believed to prevent developing thymocytes from simultaneously rearranging and expressing two TCRβ chains, whereas in DP cells the TCRα chain locus undergoes biallelic Vα-Jα rearrangement, with many possible rounds of rearrangement on each allele(Carico and Krangel, 2015, Carico et al., 2017, Genolet et al., 2012). Although the sequence of this developmental programme is the same between foetal and adult αβT-cell development, progression beyond the DN3 stage is less tightly linked to TCRβ expression in the foetal thymus(Hager-Theodorides et al., 2007).

There are several other fundamental differences between adult and foetal thymus that may affect the generation and selection of the TCR repertoire. In contrast to adult αβT-cells which are produced in a thymus structure that is mature, during foetal T-cell development, the thymus is still forming: the structure of the medulla and differentiation of the medullary thymic epithelial cell (mTEC) population, which express tissue restricted antigens for tolerance induction, are dependent on the haematopoietic compartment, with different requirements in foetal and adult thymus(Desanti et al., 2012). There are also differences in the progenitor cells that seed the thymus at different life-stages(Ramond et al., 2014), which arise from either the foetal liver or postnatal bone-marrow, and enter the thymus through different locations(Montecino-Rodriguez and Dorshkind, 2023). Some foetal haematopoietic stem cells (HSC) have been shown to have increased capacity to proliferate and to differentiate preferentially into innate-like lymphocytes compared with adult cells(Beaudin et al., 2016). Additionally, CD8 T-cells derived from HSCs from the foetal liver are functionally distinct from adult CD8 T-cells(Wang et al., 2016).

The foetal TCR repertoire is known to be less diverse than the adult repertoire. TdT is absent from the foetal thymus, and is first expressed a few days after birth, so foetal repertoires contain less non template nucleotide additions(Bogue et al., 1992). This has been confirmed by next generation TCR sequencing from mouse and human foetal and adult repertoires, which showed increased diversity after birth that was attributed to the postnatal increase in non-template nucleotide additions(Sethna et al., 2017, Britanova et al., 2016, Pogorelyy et al., 2017).

In this study we compared the TCR repertoire that is generated and selected in the foetal thymus with that from the young adult thymus. In addition to the reduction in non-template nucleotide additions seen in the embryonic repertoire, we identified biases in VJ usage and VxJ pairing of both TCRβ and TCRα repertoires. The foetal TCRβ repertoires were less diverse and less equally distributed with more clonal expansions than the young adult repertoires.

Results

Foetal thymocyte populations show clonotypic TCRβ expansion with a less diverse TCRβ repertoire and more unequal repertoire distribution than adult

To compare the TCRβ chain repertoire generated in the embryonic and young adult thymus we FACS-sorted DP (CD4+CD8+), SP4 (CD4+CD8-CD3+) and SP8 (CD4-CD8+CD3+) populations from E18.5 (foetal) and 4 week-old (young adult) thymus and sequenced their rearranged TCR transcripts. After RNA extraction from purified populations we used a TCR sequencing protocol and analysis pipeline which includes single-strand DNA ligation that tags each molecule of TCR α- and β-chain mRNA with a unique molecular identifier (UMI), allowing PCR bias to be corrected for in later analysis(Oakes et al., 2017, Uddin et al., 2019, Thomas et al., 2013). Firstly, to visualise the frequency distribution of the TCRβ repertoire in each population, we plotted the TCRβ abundance (number of copies of each sequence) against their proportion of the repertoire (Fig.1A). For each of the developmentally-defined

thymocyte populations, the foetal thymus showed an increase in the proportion of abundant clones compared to adult mice in DP, SP4 and SP8 populations (Fig.1A). The frequency distributions of TCRβ abundances were fitted to a discrete power law, where the power law exponent corresponds to the gradient on the log-log plots (Fig.1A). The power law exponent was significantly lower in each foetal population compared to its adult counterpart (Fig.1B), demonstrating a difference in distribution of abundance of TCRβ clones between foetal and adult, consistent with an increase in clonotypic expansion of abundant clones in the foetal TCRβ repertoire. To confirm this, we calculated the proportion of the TCRβ repertoire represented by the top 1% most abundant TCRβ clones in each population. In foetal DP and SP4 populations the proportion of the TCRβ repertoire represented by the top 1% most abundant TCRβ clones was more than twice that of the adult populations (Fig1C), whereas the mean abundance of TCRβ sequences detected in the top 1% most abundant (expanded) clones was significantly higher in the foetal SP4 population only, suggesting a difference in equality of distribution in the top 1% most abundant (expanded) clones in the DP and SP8 populations compared to SP4 (Fig.1D).

We therefore calculated standard indices of diversity, richness and distribution: Shannon entropy and the Gini index. Shannon entropy is derived from information theory and represents the complexity of the system, taking into account both the number of unique clonotypes and the frequencies of each clonotype, to generate a measure of richness and diversity(Shannon and Weaver, 1949). For each thymocyte population, the Shannon entropy was higher in the young adult TCRβ repertoire than in the foetal, demonstrating a richer more diverse repertoire in the adult thymocyte populations (Fig1E-F). The Gini index is a measure of the equality (evenness) of the distribution, and is frequently used in economics to demonstrate the distribution of a population's wealth, where a lower index represents a more equal distribution(Ceriani and Verme, 2012). The Gini index of the distribution of TCRβ clonotypes was significantly lower in each adult population compared to its foetal

counterpart, confirming a more equally distributed TCRβ repertoire in the young adult thymus (Fig1G-H).

In parallel we analysed the repertoire diversity, richness and distribution of the TCRα repertoires (SFig1). The fitted power law exponent of the frequency distribution of TCRα abundances was significantly lower in the foetal DP population compared to adult DP (SFig1A-B). However, we detected no significant differences between foetal and adult populations in the proportion of the TCRα repertoire represented by the top 1% most abundant TCRα clones (Sfig1C); the abundance of TCRα sequences detected in the top 1% most frequent (expanded) clones (SFig1D); the Shannon entropy (SFig1E-F); and Gini index (SFigG-H).

Foetal and young adult TCRβ and TCRα repertoires use distinct TRAV, TRAJ, TRBV and TRBJ gene segments

We next tested if the foetal and young adult repertoires showed differences in usage of TCR V and J gene segments. We found many differences between foetus and adult in proportional V and J segment usage within unique TCRβ and TCRα sequences for DP (SFig2), SP4 (SFig3) and SP8 (SFig4) populations. Preferential gene segment usage according to life-stage appeared to correlate with the chromosomal location of the gene segment, particularly for TRAV and TRBV usage within the DP population, where the adult repertoire favoured the 5' gene segments, and the foetus the 3' gene segments. To visualise these differences, we plotted heatmaps of mean proportional gene segment usage for unique TCR sequences, clustering each life-stage and thymocyte population, but showing each gene segment in chromosomal order (Fig2A-D). The samples clustered by life-stage first before cell-type (E18.5 populations clustered together) for both TCRα and TCRβ, suggesting that VJ gene usage is altered in the foetus compared to young adult. Interestingly, both TRAV and TRAJ showed clear preference for chromosomal location, with foetal populations favouring 3' TRAV segments and 5' TRAJ segments, whereas adult populations showed enrichment of 5' TRAV and 3' TRAJ (Fig2A-B). To test if this bias in gene usage was present in the unselected TCRα

repertoire, we separated the DP population into cells that have not yet entered positive selection ($CD3^{-/lo}DP/CD69^{-}DP$) and cells that have entered TCR repertoire selection ($CD3^{+/hi}DP/CD69^{+}DP$). Both foetal DP populations clustered together and showed similar bias towards 3' TRAV and 5' TRAJ, suggesting that the bias was independent of positive selection. In the case of the adult DP populations, however, the more immature DP population clustered separately from the other young adult populations and showed weaker enrichment for 5'TRAV and 3'TRAJ than the populations that had undergone or were undergoing positive selection ($CD3^{+/hi}DP$, SP4 and SP8). This suggests that in the adult thymus, positive selection changes proportional TRAV and TRAJ gene usage, whereas in the foetal thymus an inherent bias in VJα gene usage persists after positive selection.

Heatmaps for TRBV and TRBJ also broadly showed chromosomal location-bias for gene usage at the different life-stages, with foetal populations preferentially using 3'TRBV and 5'TRBJ, although the pattern appeared less pronounced (Fig2. C-D). Therefore, to evaluate further the differences in TCRβ gene segment usage between foetal and adult repertoires, we carried out Principal Component Analysis (PCA) of the β-chain variable and joining gene counts of the unique TCRβ chains for each population (Fig. 2E-G). PCA separated the repertoires for DP, SP4 and SP8 by life-stage on PC1, confirming differences in TRBV and TRBJ usage between life-stage for each population.

Foetal and adult TCRβ and TCRα repertoires use distinct combinations of V and J segments

Given this difference in TRBV and TRBJ gene usage between foetal and adult, we next tested if TCRβ foetal and young adult thymocyte repertoires use different combinations of V and J gene segments. We carried out PCA using the counts of each VxJ combination from unique TCRβ sequences in foetal and adult DP, SP4 and SP8 populations (Fig3A-B). PCA separated by life-stage on PC1, with all adult repertoires clustering tightly together (Fig3A). When we compared by thymocyte population, each adult population clustered together, with adult SP4 separating from adult SP8 on PC2, and DP cells scoring in between, suggesting that PC2 might

correspond to MHC-restriction of the adult populations (Fig3B). In contrast, the foetal populations were more dispersed, and did not segregate fully by cell type on PC2 (Fig3B). When we examined which VxJ combinations contributed most to PC1, we found strong correlation to the proportional TRBV and TRBJ usage detected: TRBV13-1 and TRBJ2-7 both showed adult bias in the analysis of individual gene usage, and in combination also contributed strongly to the positive score on PC1; whereas TRBV20 and TRBJ1-3 both showed foetal bias in the analysis of individual gene usage and contributed strongly to the negative (foetal) score on PC1, reflecting chromosomal gene segment location (SFig2-4 and Fig2-D).

We next compared usage of all possible VxJ combinations between the adult and foetal thymocyte populations for both TCRβ and TCRα repertoires, identifying all combinations that showed a significant change in proportional usage in foetus compared to young adult (Fig4A-C). The DP foetal population showed many increases (shown in red) and decreases (shown in blue) in proportional usage of VxJ combinations for TCRβ repertoire compared to young adult, which after selection were reduced in the SP populations. In the case of the TCRα chain, the foetal DP repertoire favoured VxJ combinations from the 3' location of TRAV and 5' location of TRAJ, but this bias was less pronounced in the SP populations (Fig.4B-C). Concomitantly, the DP foetal population showed clear proportional decrease in usage of combinations of 5' TRAV and 3' TRAJ in comparison to young adult.

Shorter CDR3 length and reduced non-template insertion length in foetal TCRβ repertoires

We next tested if the percentage of non-productive TCRβ rearrangements was different in foetal and young adult populations. The proportion of non-productive rearrangements was higher in the foetal SP8 population than adult (Fig5A). Furthermore, we examined non-template additions/deletions to V and J gene segments, which in the TCRβ chain include TRBD nucleotides. TRBD segments are difficult to identify as they are highly homologous and short. As previously reported(Sethna et al., 2017), the mean TCRβ non-template nucleotide insertion length was lower in the foetal DP and CD4SP populations compared to adult. To

confirm this we then investigated the length of the complementary determining region 3 (CDR3) of the TCRβ chain as it is the most hypervariable region and primary site of antigen recognition. The mean predicted CDR3 length was shorter in all three populations in foetal TCRβ repertoires compared to young adult, confirming previous studies(Sethna et al., 2017) (Fig5B-C).

In contrast, when we compared predicted amino acid CDR3 sequences for the TCRα repertoires, we found no significant differences in the percentage of non-productive TCRα rearrangements between each adult and foetal population, or in the mean length of non-template insertions (SFig5A-B). The mean α-chain CDR3 length, however, was greater in the adult DP population than in foetal DP population (SFig5C).

Sharing of CDR3 sequences and CDR3 sequential amino acid triplets (k-mers) differs between adult and foetal TCRβ and TCRα repertoires.

In order to investigate sharing between the predicted CDR3 repertoires within the same cell population from different embryos/mice of the same life-stage, we used the Jaccard Index of Similarity. This index measures the size of the intersection divided by the size of the union of finite sample sets(Jaccard, 1912). We calculated the Jaccard Index of Similarity for each CDR3 repertoire from each thymocyte population, comparing different mice/embryos to determine how similar each foetal repertoire is to the repertoire of the same thymocyte population from another foetus, and likewise for young adults. For each population, the Jaccard index was significantly higher in the foetal samples compared to adult, indicating that the CDR3 repertoires in each population from different embryos shared more sequences than the CDR3 repertoires from different individual adults (Fig5D-E). This increased sharing of CDR3 sequences in the foetal repertoires is consistent with shorter CDR3 length and shorter non-template insertions, leading to a repertoire that contains more genomic sequence than adult. We then compared the similarity in β-chain sequential CDR3 amino acid triplets (k-mers) for each population in the foetus and the adult. Conserved sequential amino acid triplets play an

important role in determining antigen specificity and can aid in clustering together CDR3s that have similar specificities (Thomas et al., 2014, Glanville et al., 2017). Although the foetal repertoires from different individuals shared more CDR3 sequences with one another in all three populations than the adults, the adult populations shared more sequential motifs within their CDR3s with one another in DP and SP8 than the foetal populations (Fig5G-H). In support of this, when we carried out PCA, using the frequency distributions (counts) of each k-mer within CDR3 as input, the adult populations clustered together tightly scoring positive on PC1 and negative on PC2, whereas the foetal samples were more dispersed (Fig5I-J). Given that the foetal CDR3 repertoires contained fewer non-template nucleotides and showed more CDR3 sharing than adult, the increased adult CDR3 amino acid motif sharing is likely to be the result of selection of recurrent motifs by contact with pMHC during positive selection. In the case of the α-chain repertoires, we did not detect differences in life-stage sharing of TCRα predicted CDR3 sequences between individuals (SFig5D-E), but we found the adult DP, SP4 and SP8 repertoires shared more CDR3 amino acid triplets (k-mers) between one another than the foetal populations (SFig5F-G). However, in PCA, using the frequency distributions (counts) of each k-mer within the TCRα CDR3 as input, although most adult samples clustered together, the samples failed to segregate on either PC1 or PC2 by life-stage or by population (SFig5H-I).

Different CDR1 and CDR2 usage between foetal and adult TCRβ and TCRα repertoires

The CDR1 and CDR2 loops in the TCR are encoded in the V gene segments and typically contact the MHC's conserved α-helices. They can determine MHC restriction during repertoire selection(Wong et al., 2019), so we examined CDR1xCDR2 combinations in the foetal and adult thymocyte populations. We carried out PCA, using the frequency distributions (counts) of each β-chain CDR1xCDR2 combination as input (Fig6A-C). The PCA clustered the populations by life-stage and cell-type, with the DP samples positioning between either SP population. To further visualise this, we generated a heatmap of the proportional usage of β-

chain CDR1xCDR2 combinations for each foetal or adult thymocyte population (Fig. 6D). The foetal populations clustered together, showing preference for distinct CDR1xCDR2 combinations, which reflect the bias observed in their TRBV gene usage (Fig 2C). For both foetal and adult samples, DP populations were positioned between SP8 and SP4, suggesting a divergence in CDR1xCDR2 usage as a result of MHC restriction following positive selection. Indeed, referring back to the PCA (Fig6C), CDR1xCDR2 combinations that contributed strongly to the positive side on PC1, such as MSHET-SYDVDS (TRBV29) and SGHSN-HYEKVE (TRBV12-1), showed increased expression in SP8 and decreased expression in SP4 (consistent with MHCI-restriction), while combinations that contributed strongly to the negative side of PC1, such as NSQYPW-LRSPGD (TRBV31) and GKSSPN-SITVG (TRBV1), showed increased expression in SP4 and decreased expression in SP8 (consistent with MHCII-restriction).

TCRα CDR1 and CDR2 may also be determined by MHC-restriction(Sim et al., 1996), so we additionally investigated TCRα CDR1xCDR2 combinations in the TCRα repertoires (Fig6E). Again, samples from each life-stage grouped together, and consistent with the strong life-stage dependent influence on TRAV use, several CDR1xCDR2 combinations showed an adult-bias in usage. PCA, using the frequency distributions (counts) of each predicted α-chain CDR1xCDR2 combination as input failed to segregate samples by life-stage on either PC1 or PC2 (SFig6A-B). However, in the case of the adult samples only, PC2 separated samples by population, with SP4 cells scoring negative on PC2 and SP8 cells scoring positive, suggesting that TCRα CDR1/CDR2 usage was influenced by MHC restriction in adult repertoire selection, consistent with other reports in mouse and human(Camaglia et al., 2023, Suo et al., 2023).

Young adult DP VJα gene segment usage becomes more foetal-like after hydrocortisone treatment

We observed distinct patterns of V and J gene usage between foetus and young adult, with foetal DP repertoires showing bias towards use of 3’ V and 5’ J rearrangements (Fig2-4).

During TCRβ gene rearrangement, these segments are closest to one another in the looping structure that enables V to DJ rearrangements (Skok et al., 2007), suggesting this might account for the foetal bias in proportional TRBVxTRBJ segment usage. In contrast to TCRβ locus rearrangement, the TCRα locus can undergo multiple rounds of rearrangement on each chromosome, sequentially moving 3' to 5' along the TRAV array, while moving 5' to 3' along the TRAJ array, with proximal pairs (3' TRAV segments with 5' TRAJ segments) initiating this sequence of rearrangements(Carico et al., 2017). We observed that the foetal DP repertoire showed TRAVxTRAJ bias by their chromosomal position. One possible explanation for this bias is that in the foetus progressive rounds of TCRα rearrangement are less common than in young adult, perhaps as a result of differences in the kinetics of T-cell development. Differentiation of foetal thymocytes occurs in a largely synchronized wave, whereas adult thymocyte production is unsynchronised, continuous and slower. Once the adult thymus has reached steady-state, homeostasis between thymocyte populations regulates the rate of differentiation to DP cell (Hager-Theodorides et al., 2007, Outram et al., 2009). To examine the influence of the rate of differentiation on VJ gene usage, we synchronized the differentiation of adult DP thymocytes by treating young adult mice with hydrocortisone (HC) to deplete the adult thymus of all but the most mature cells. At 2 days after treatment, the thymus was depleted of DP cells. Four days later (6 days after treatment), we FACS-sorted and TCR sequenced the replenished $CD3^{-/lo}$DP ($CD3^{-/lo}$CD4+CD8+), and $CD3^{+/hi}$DP ($CD3^{+/hi}$CD4+CD8+) populations. We plotted heatmaps of mean proportional V and J gene segment usage for unique TCR sequences in foetal, HC-treated and control young adult repertoires, clustering each life-stage and thymocyte population, but showing each gene segment in chromosomal order (Fig7A-D). Foetal and adult HC-treated TCRα repertoires clustered together, with untreated adult repertoires clustering separately (Fig7A-B). Interestingly, both foetal and HC-treated young adult populations favoured 3' TRAV segments and 5' TRAJ segments, in contrast to control young adult populations, that displayed bias for 5' TRAV and 3' TRAJ (Fig7A-B). Therefore, by synchronizing young adult thymus using HC,

foetal and young adult gene segment usage became more alike, with 5' TRAV and 3' TRAJ bias. We next compared usage of all possible VxJ combinations between control and HC-treated young adult DP populations for all TCRα sequences, identifying combinations that showed a change in proportional usage in the HC-treated young adult compared to control young adult (Fig4A-C). The DP HC-treated young adult population favoured VxJ combinations from the 3' location of TRAV and 5' location of TRAJ along with clear proportional decrease in usage of combinations of 5' TRAV and 3' TRAJ in comparison to young adult control (Fig7C). In the case of the β-chain, analysis of proportional TRBV and TRBJ gene segment usage in unique β-chain rearrangements showed that samples clustered by life-stage first, with both untreated and HC-treated young adult repertoires clustering together (Fig7D-E). However comparison of proportional usage of all possible unique TCRβ VxJ combinations between HC-treated and control young adult DP populations showed a 5' bias in TRBJ gene segment usage (Fig7F). These data indicate that when the adult young adult DP population arises quickly and synchronously its TRAV, TRAJ and TRBJ segment usage and TRAVxTRAJ combinations closely ressemble the foetal DP repertoire, suggesting that the kinetics of transition to DP cell are important in determining gene segment usage.

Discussion

Here we employed a bulk population-based strategy to investigate the TCRβ and TCRα chain repertoires during T-cell development. This enabled us to quantify changes in repertoire diversity and distribution as thymocytes develop from DP to SP cell, and to identify differences in the TCR repertoire between foetal and young adult animals. In validation of this approach, we were able to quantify known differences in TCRβ repertoire diversity, CDR3 length and non-template insertion length between foetal and adult(Sethna et al., 2017). The foetal TCR repertoire contained fewer non-template nucleotides than adult, indicating that it was more closely aligned to genomic sequence. Consistent with this, the predicted foetal β-chain CDR3 repertoires shared more sequences with one another than their young adult counterparts. Our study also showed that the foetal TCRβ repertoire had a less equal distribution in DP, SP4 and SP8 populations compared to adult, and increased clonal expansion of the most abundant clones in DP and SP4 populations. Thus, the reduction in TCRβ repertoire diversity observed in the foetal thymus could not simply be attributed to the reduction in N-nucleotide insertions. These differences in TCRβ repertoire distribution and clonal expansion may be the result of differences in the kinetics of expansion and differentiation of thymocyte subsets in the foetus, leading to greater clonal expansion of TCRβ clones following β-selection. The transition from DP to SP cell in the foetus takes just 2-3 days at most, as DP cells first appear around E16, and the mature SP populations were FACS-sorted on E18.5, whereas in the adult thymus differentiation from DN3 to SP cell may be slower(Ross et al., 2014, Solanki et al., 2020).

We found many differences in proportional TRBV, TRBJ, TRAV, and TRAJ gene usage between foetal and adult thymocyte populations, with foetal populations showing proportional bias towards 3' TRBV and 5'TRBJ usage. We observed a particularly striking bias towards use of 3' TRAV and 5' TRAJ gene segments in the foetus. In mammals, the gene segments encoding TCRδ and TCRα chains are found at a single genetic locus, with TCRδ rearrangement taking place at the DN stage of development (prior to TCRα rearrangement in the αβ-lineage

committed DP population). The TCRα locus can undergo multiple rounds of rearrangement on each chromosome, with proximal pairs (3' TRAV segments with 5' TRAJ segments) initiating this sequence of rearrangements. However, as TCRδ gene segments are nested between the TRAV and TRAJ array and also amongst the TRAV array, TCRδ gene rearrangement splices out 3' TRAV segments, facilitating 5' TRAV segment pairing with TRAJ segments(Carico et al., 2017). It is therefore possible that the 3' TRAV and 5' TRAJ bias observed in the foetus may in part be the result of primary TCRα rearrangements taking place on chromosomes which have not already rearranged TCRδ, so that 5' TRAV segments are not favoured. In the future, it will be important to test experimentally if the combination of 3' TRAV segments with 5' TRAJ segments contribute to TCRs which facilitate functions associated with foetal T-cells, as this might account for the evolutionary conservation of the genomic organization of the TCRα and TCRδ loci across mammals.

Bias in TCRα gene segment usage by chromosomal location has been reported in human DN thymocyte populations by single cell RNAseq but was found to diminish as thymocytes mature and progressive recombination of the TCRα loci occurs(Park et al., 2020). In contrast, in the mouse foetal thymus, we found that the bias in proportional TRAV and TRAJ gene segment use by chromosomal position persisted in the positively selecting $CD69^{+}$DP and mature SP4 populations, but was not apparent in the adult $CD3^{-/lo}$DP population. Our data therefore suggest that progressive rounds of TCRα rearrangement are less common in the foetal DP population. Indeed, when we depleted the young adult thymus by HC-treatment, we found an increase in 3'TRV and 5'TRJ gene segment usage in the recently differentiated recovering DP population, making these repertoires more similar to the foetal DP TCRα repertoires. In support of this, the VJ gene usage of HC-treated young adult DP populations clustered together with foetal. Thus differences between foetal and control young adult TCRαV-J rearrangements in DP cells may be the result of slower differentiation in the adult thymus, allowing more time for multiple rounds of TCRαV-J rearrangements in the DP population.

Consistent with this, the foetal DP population showed a different TCRα frequency distribution than the adult DP population, with a lower power law exponent.

Comparison of proportional use of TCRβVxJ and TCRαVxJ combinations between adult and foetal populations also highlighted the 3' V gene segment preference in the foetal DP population, and the 5' V gene segment preference in the adult DP population for both β-chain and α-chain. Interestingly, life-stage had a greater impact on TCRβ and TCRα gene segment usage than MHC-restriction in all populations.

PCA clustered β-chain VxJ combination counts by population in the adult samples, showing the impact of MHC restriction (positive selection) on the selected adult SP repertoires. PCA also clustered the adult counts of β-chain CDR1xCDR2 combinations by cell type, confirming impact of MHC restriction on Vβ gene usage. However, foetal populations failed to segregate fully by cell type in either PCA, suggesting that MHC restriction/positive selection has less influence on β-chain V and J gene segment use in the foetal SP populations. In support of this, young adult β-chain CDR3 repertoires shared more sequential amino acid motifs (k-mers) than foetal repertoires, suggesting a stronger influence of pMHC on adult repertoire selection.

In the case of the TCRα repertoire the DP population showed many increases in proportional use of 3'TRAV and 5'TRAJ combinations in the foetal thymus, whereas the adult DP population showed clear proportional bias to 5'TRAV to 3'TRAJ combinations. PCA clustered the adult α-chain CDR1xCDR2 combinations by cell type, confirming impact of MHC restriction on Vα gene usage in the SP populations. However, as also observed in the analysis of β-chain repertoires, the foetal samples did not cluster by cell-type, suggesting a weaker influence of MHC-restriction/positive selection on both the TCRβ and TCRα repertoires that are selected in the foetal thymus.

In summary, our study revealed many differences between the foetal and young adult TCR repertoire diversity, distribution, CDR3 length, and gene segment usage by bulk sequencing separate TCRβ and TCRα repertoires from developmentally defined thymocyte populations.

Taken together, these data suggest that MHC restriction and positive selection have a weaker impact on the TCR repertoire in foetal thymus compared to adult. Overall, the differences between the foetal and adult thymus TCR repertoires are consistent with the foetal thymus producing αβT-cells with properties and functions that are distinct from adult T-cells, and more innate-like: their repertoire is less diverse, more closely encoded by genomic sequence, less governed by MHC-restriction, and with preference for particular gene segment usage. Several recent studies have demonstrated distinct and more innate-like features of foetal and neonatal T-cell populations in both humans and mice (Beaudin et al., 2016, Wang et al., 2016, Rackaityte and Halkias, 2020, Smith et al., 2018). The first wave of foetal αβT-cells that leave the thymus must provide early protection against infection in the neonatal animal but also need to be tolerant to both self and maternal MHC/antigens. It is possible that the distinct features and weaker MHC-restriction of the foetal TCR repertoire have evolved to provide these two important features of foetal adaptive immunity. It will be interesting to investigate if the foetal-bias in gene segment usage confers specific properties on foetal TCRs, with respect to their binding specificity, affinity and avidity.

Our approach of bulk TCR sequencing from FACS-sorted thymocyte populations had the advantages of scale (allowing the sequencing of thousands of rearrangements from thousands of cells from each embryo or mouse), at relatively low cost. However, it had the disadvantage that we were unable to investigate which TCRβ rearrangements pair with which TCRα rearrangements in single cells. Clearly, in future it will be important and interesting to expand this analysis to include TCRβ/α pairing by single cell RNAseq.

Materials and methods

Mice

C57/BL6 mice were bred and maintained in specific pathogen-free conditions at University College London (UK) under UK Home Office regulations. For hydrocortisone (HC) treatment,

mice were injected intraperitoneally with 0.6mg/gram of body weight pure HC sodium phosphate (Sigma Aldrich, cat. no: BP188) in sterile PBS, and analysed after 6 days.

Fluorescence activated cell sorting

Each foetal or young adult thymus was disaggregated into a single cell solution using the back of a syringe on a 70-M cell strainer. The cells were washed through the filter into falcon tubes using ice cold FACs buffer (1x AIM-V medium (research grade), AlbuMAX Supplement (Gibco, cat. no: 31035025)) to eliminate any large clumps. Cells were then counted using Accuri C6 flow cytometer and then pelleted by centrifugation for 5 minutes at 1400 rpm and supernatant was removed. The whole cell pellet from the entire organ was stained with a panel of directly conjugated antibodies supplied by Biolegend (San Diego, US) or eBioscience (San Diego, US). See Supplementary Table 1 and 2 for antibody panels. Firstly, an antibody mastermix of either 1:50 (foetal thymus) or 1:100 (adult thymus) in fresh ice cold FACS buffer was prepared. Subsequently, either 100 µL (foetal thymus), 400 µL (adult thymus) of antibody mastermix was then added to pelleted cells and the cells were then stained on ice for 30 minutes in the dark. The stained cells were then washed using 2 mL of FACS buffer and pelleted by centrifugation for 5 minutes at 1400 rpm. The cells were resuspended in either 100 µL (foetal thymus), or 500 µL to 1 mL (thymus) of fresh ice cold FACS buffer depending on the cell counts. To obtain $CD3^{-/lo}$DP ($CD4^{+}CD8^{+}CD3^{-/lo}$), $CD69^{-}$DP ($CD4^{+}CD8^{+}CD69^{-}$), $CD69^{+}$DP ($CD4^{+}CD8^{+}CD69^{+}$), $CD3^{+/hi}$ DP ($CD4+CD8+CD3^{+/hi}$), SP4 ($CD4^{+}CD8^{-}CD3^{+}$), SP8 ($CD4^{-}CD8^{+}CD3^{+}$) thymocyte cell suspensions were sorted using a BD FACS Aria III. CD69 expression was used to differentiate DP populations in the foetus, as anti-CD3 staining is dull in DP thymocyte populations at E18.5(Solanki et al., 2018). Only live cells were gated and collected using forward and side scatter.

The cells were collected in 100 µL (foetus) or 400 µL (young adult) of FACS buffer and were then pelleted by centrifugation for 25 minutes at 1400 rpm at 4 °C. The supernatant was

removed and 100 µL of Extraction buffer from PicoPure RNA isolation kit (Applied Biosystems, cat. no. KIT0204) was added. Finally, the samples were incubated for 30 minutes at 42 °C on a shaking heatblock and then stored at -80 °C until the RNA was ready to be extracted.

RNA extraction

RNA was extracted by PicoPure RNA isolation kit (Applied Biosystems, cat. no. KIT0204) according to manufacturer's instructions and eluted in 11 µL of elution buffer. RNA concentration was assessed using a spectrophotometer.

TCR amplification and sequencing

We used the protocol for TCR amplification and sequencing as described (Oakes et al., 2017, Uddin et al., 2019), with some minor modifications for mouse samples. See Supplementary Table 3 for the primer list with the sequences and Supplementary Table 4 for a full list of reagents.

RNA was first DNase treated. A maximum of 500 ng of RNA was mixed with 1 µL RQ1 10x Buffer (Promega, cat. no: M6101) and 1 µL RQ1 DNase (1 U/µL, Promega, cat. no: M6101) and then incubated at 37 °C for 30 minutes. 1 µL of RQ1 DNase Stop Solution (Promega, cat. no: M6101) was then added and the mix was incubated at 65 °C to stop the reaction. The RNA was then reverse transcribed by adding 1.5 µL of 10 µM TRAC2 primer, 1.5 µL of 10 µM TRBC3 primer, and 1.5 µL of 10 mM dNTPs (Promega, cat. no: U1515) and incubating at 65 °C for 5 minutes. The reaction was then rapid cooled down on ice and 6 µL of 5x FS Buffer (Invitrogen, cat. no: 18080044), 1.5 µL of 0.1 M DTT (Invitrogen, cat. no: 18080044), 1.5 µL of RNasin Ribonuclease Inhibitor (40 U/µL, Promega, cat. no: N2111) and 1.5 µL of SuperScript III RT (200 U/µL, Invitrogen, cat. no: 18080044) was added and it was incubated at 55 °C for 30 minutes, followed by 70 °C for 15 minutes. These reactions were purified by Minelute PCR purification (Qiagen, cat. no: 28004) following the manufacturer's instructions and eluted in 10.5 µL nuclease-free water.

The cDNA was then ligated to the M13 ligation primer which is composed of the Illumina SP2 primer, an 8 base spacer and a 12 base Unique Molecular Identifier (UMI). This UMI consists of two random hexamers separated by the 8 base spacer. On the 5' end the primer is phosphorylated, and on the 3' end it is blocked with a Spacer C3 moiety to prevent primer concatemerization. The ligation mix consisted of: 10 µL cDNA, 3 µL of bovine serum albumin (BSA)/hexamine cobalt chloride (HCC) mixture (1 mg/mL BSA, 10 mM HCC), 3 µL of T4 RNA ligase buffer (NEB, cat. no: M0204S), 1 µL of 10 mM ATP (NEB, cat. no: M0204S), 1 µL of 10 µM M13 Ligation primer, 2 µL of T4 RNA Ligase (10 000 U/mL, NEB, M0204S), and 10 µL of PEG 8000 50% (NEB, cat. no: M0204S). The ligation mix was then incubated for at least 18 hours up to a maximum of 23 hours at 16 °C and then heat inactivated at 65 °C for 10 minutes. 70 µL of nuclease-free water was added to the ligation products. This was then purified by adding 50 µL of AMPure XP Beads (Beckman Coulter, cat. no: A63881) to the 100 µL ligation product, with some modifications to manufacturer's instructions: 300 µL of 80% ethanol was used for the washing steps and the product was eluted in 31 µL nuclease-free water.

The purified ligation product was then amplified in a PCR reaction consisting of 31 µL purified product, 10 µL of 5x HF Buffer (NEB, cat. no: M0530L), 2.5 µL of 10 µM m- alpha-RC1 primer, 2.5 µL of 10 µM m-beta-RC1 primer, 2.5 µL of 10 µM SP2-M13 primer, 1 µL of 10 mM dNTPs (Promega, cat. no: U1515), and 0.5 µL of Phusion Polymerase (NEB, cat. no:M0530L). The m-alpha-RC1 and m-beta-RC1 primers hybridize to the constant region of the α-chain and β -chain genes in the mouse respectively. The SP2-M13 primer hybridizes to the sequence introduced by the M13 ligation primer earlier during the ligation step. PCR-1 was run using the following conditions: initial denaturation at 98°C for 3 minutes, followed by 4 cycles of denaturation at 98°C for 15 seconds, annealing at 69°C for 30 seconds and extension at 72°C for 40 seconds, followed by a final extension at 72°C for 5 minutes.

The 50 µL PCR product was then purified by adding 40 µL of AMPure XP Beads (Beckman Coulter, cat. no: A63881) with some modifications to manufacturer's instructions: 200 µL of

80% ethanol was used for the washing steps. At this stage the samples were split into two: TCRα and TCRβ, each eluted in 31 µL nuclease-free water.

The purified PCR product was then amplified in a PCR reaction to add indices and Illumina adaptors P5 and P7 and sequencing primer 1 (SP1) sequence. The PCR reaction mix consisted of: 31 µL purified product, 2.5 µL of 1 µM SP1 index (mSP1- 6N-I-**X**-αRC1 or mSP1-6N-I-**X**-βRC1, for TCRα and TCRβ respectively), 2.5 µL of 10 µM SP2 index (P7-L**X**), 2.5 µL of 10 µM SP1-P5 primer, 10 µL of 5x HF Buffer (NEB, cat. no: M0530L), 1 µL of 10 mM dNTPs (Promega, cat. no: U1515), and 0.5 µL of Phusion Polymerase (NEB, cat. no: M0530L). PCR-2 was run using the following conditions: initial denaturation at 98°C for 3 minutes, followed by 6 cycles of denaturation at 98°C for 15 seconds, annealing at 69°C for 30 seconds and extension at 72°C for 40 seconds, followed by a final extension at 72°C for 5 minutes. The 50 µL PCR product was then purified by adding 40 µL of AMPure XP Beads (Beckman Coulter, cat. no: A63881) with some modifications to manufacturer's instructions: 200 µL of 80% ethanol was used for the washing steps, and the product was eluted in 30 µL nuclease-free water.

The purified PCR product was then amplified in a qPCR reaction, so that the reaction can be monitored and stopped in real time when the reaction passes the threshold of 0.1 ΔRn to prevent overamplification and minimise the introduction of PCR artifacts. SYBR Green I Nucleic Acid Gel Stain, 10,000x concentrate in DMSO (ThermoFisher Scientific, cat. no: S7567) was diluted firstly 1:100 in DMSO and this stock solution was stored at -20 °C. Prior to the assembly of the PCR mix, this stock solution was diluted a further 1:50 in nuclease-free water. The PCR reaction consisted of: 28 µL purified product, 10 µL of 5x HF Buffer (NEB, cat. no: M0530L), 5 µL of SYBR Green (1:50), 1.25 µL of 10 mM dNTPs (Promega, cat. no: U1515), 1 µL of Rox (Invitrogen, cat. no: 12223012), 2.5 µL of 10 µM P5 primer, 2.5 µL of 10 µM P7 primer and 0.5 µL of Phusion Polymerase (NEB, cat. no: M0530L). The qPCR was run using the following conditions: initial denaturation at 98°C for 3 minutes, followed by a variable number of cycles of denaturation at 98°C for 15 seconds, annealing at 69°C for 30 seconds and extension at 72°C for 40 seconds, followed by a final extension at 72°C for 5 minutes.

The reaction was stopped when the samples passed the threshold of 0.1 ΔRn. The 50 µL PCR product was then purified by adding 40 µL of AMPure XP Beads (Beckman Coulter, cat. no: A63881) with some modifications to manufacturer's instructions: 80% ethanol was used for the washing steps and the product was eluted in 30 µL nuclease-free water.

The purified products were then quantified using Qubit dsDNA high sensitivity reagents (ThermoFisher Scientific, cat. no: Q32854) and the size was confirmed with the TapeStation System HSD1000 (Agilent, cat. no: 5067-5584, cat. no: 5067-5585). The expected size is around 650 bp for a successful library preparation.

Sequencing

The concentrations acquired by the Qubit and the size determined by the TapeStation, were used to calculate the molarity of the samples in nM. The samples were then diluted to 12 nM and pooled into one 12 nM library containing samples with different indices. 84 samples were prepared per sequencing run (42 α-chain and 42 β -chain libraries). A Vacuum Concentrator Centrifuge was used to pellet the library and remove excess volume, so that 30 µL of the pooled library could then be run on the Pippin Prep System using a Pippin Gel Cassette 1.5% w/v agarose dye free 250 bp-1.5 kb DNA size range (Sage Science, cat. no: CDF1510) to size select for sequences between 350 to 750 bp, following the manufacturer's instructions.

40 µL of library eluted from the Pippin Prep was then quantified using a Qubit and TapeStation System HSD1000 as detailed above. The expected molarity was between 2 nM and 5 nM. The library was then denatured and diluted to 1.2 pM according to standard Illumina's protocols (for 4 nM libraries) and was spiked with 22% of 20 pM PhiX control (Illumina, cat. no: FC-110-3001). The 1.2 pM library was sequenced on the NextSeq using the NextSeq 500/550 Mid Output Kit v2.5 (300 Cycles) (Illumina, cat. no: 20024905) at UCL genomics.

Error correction and outputting

The NextSeq outputs files in the format named binary based call (.bcl) which were converted into FASTQ files using bcl2fastq for downstream processing using a pipeline of scripts described previously(Oakes et al., 2017, Thomas et al., 2013): *Decombinator_v3.1* (available at: https://github.com/innate2adaptive/Decombinator/) in Python 2.7. This pipeline identifies the errors introduced by PCR amplification using the UMI attached during the ligation step and thus produces an output of a corrected abundance of the TCR in the sample along with determining V, J and CDR3 regions for each TCR.

Downstream analysis

For further downstream analyses, *R Studio* was used. The *tidyverse* set of packages were used for data manipulation and visualisations, in particular *ggplot2*(Wickham, 2016, Wickham H, 2019). Dotplots show mean±c.i (package *ggpubr*(Kassambara, 2023a)) and statistical comparisons were carried out by unpaired Student's t-test or Welch's t-test as appropriate using the package *rstatix(Kassambara, 2023b). Pheatmap* and *ComplexHeatmap* were used to generate Pearson correlation heatmaps(Gu et al., 2016, Kolde, 2019).

TCR abundance distribution

TCR repertoire abundance distributions are typically L-shaped, with a high number of distinct TCRs or clonotypes present only once, and a low number of hyperexpanded clones. Therefore, the TCR abundance (number of copies of each sequence) was plotted against their proportion of the repertoire in a log-log plot. This transformed distribution follows approximately a linear distribution apart from the largest clones and can be fitted to a discrete power law ($f(x) = kx^{-\alpha}$) as seen in previous studies(Oakes et al., 2017, Joshi et al., 2019). The TCR abundance frequency was fitted to a discrete power law using maximum likelihood estimation(Bauke, 2007, Clauset et al., 2009) using the *PoweRLaw* package(Gillespie, 2015). The power law exponents (α) were then plotted and compared.

Diversity indices

Before calculating diversity indices, α and β identified TCRs or CDR3s were subsampled (rarefied) to a number lower than the smallest repertoire using the package *vegan*(Oksanen et al., 2022) in order to correct for differences in diversity due to sample size. The mean diversity indices (Shannon Entropy, Gini Index and Jaccard Index of Similarity) were then calculated from 1000 repeats of this random sampling. The Shannon Entropy was computed using the package *vegan*(Oksanen et al., 2022). Gini index was computed using *ineq* package(Zeileis, 2014). The base R function *dist* was used to calculate the Jaccard Index of Similarity.

Principle Component Analysis

Before PCA was applied, raw counts were first $\log_{10}$ transformed to account for differences in sample size, using a pseudocount of 0.01 for any counts that were not observed. Z-scores were then calculated from these values by subtracting the mean and dividing by the standard deviation. PCA was then computed using the base R function *prcomp* and *factoextra* package was used to investigate the results(Kassambara A, 2020).

VxJ combinations

Proportional VxJ gene usage of total TCRs was calculated for each sample and only VxJ combinations that were detected in all samples were compared. Statistical comparisons were carried out by unpaired Student's t-test followed by FDR-adjustment (5%, Benjamini-Hochberg procedure) of *p* values.

Sequential amino acid triplet analysis

Conserved sequential amino acid triplets (k-mers) can be important in determining antigen specificity and can help cluster CDR3 sequences according to specificity (Thomas et al., 2014,

Glanville et al., 2017) and were extracted from the predicted amino acid CDR3 sequences using the *immunarch* package(Team, 2019).

Authors' Contributions

JR, BC and TC conceived the study; JR and TC designed experiments and wrote the manuscript. JR analysed sequencing data; JR, C-IL, DY and SR performed experiments. C-IL and BC critically reviewed the manuscript.

Acknowledgements

This work was funded by the MRC (MR/P000843/1); MR/S037764/1) and BBSRC (BB/T020970/1). JR was supported by a studentship from the BBSRC London Interdisciplinary Biosciences Consortium (1903458). Research at UCL Great Ormond Street Institute of Child Health is supported by the NIHR Biomedical Research Centre at Great Ormond Street Hospital and UCL. The authors declare no competing financial interests.

Data Availability

TCR sequencing data will be made available on UCL Research Data Repository.

References

BAUKE, H. 2007. Parameter estimation for power-law distributions by maximum likelihood methods. *The European Physical Journal B,* 58**,** 167-173.

BEAUDIN, A. E., BOYER, S. W., PEREZ-CUNNINGHAM, J., HERNANDEZ, G. E., DERDERIAN, S. C., JUJJAVARAPU, C., AASERUDE, E., MACKENZIE, T. & FORSBERG, E. C. 2016. A Transient Developmental Hematopoietic Stem Cell Gives Rise to Innate-like B and T Cells. *Cell Stem Cell,* 19**,** 768-783.

BOGUE, M., GILFILLAN, S., BENOIST, C. & MATHIS, D. 1992. Regulation of N-region diversity in antigen receptors through thymocyte differentiation and thymus ontogeny. *Proc Natl Acad Sci U S A,* 89**,** 11011-5.

BRITANOVA, O. V., SHUGAY, M., MERZLYAK, E. M., STAROVEROV, D. B., PUTINTSEVA, E. V., TURCHANINOVA, M. A., MAMEDOV, I. Z., POGORELYY, M. V., BOLOTIN, D. A., IZRAELSON, M., DAVYDOV, A. N., EGOROV, E. S., KASATSKAYA, S. A., REBRIKOV, D. V., LUKYANOV, S. & CHUDAKOV, D. M. 2016. Dynamics of Individual T Cell Repertoires: From Cord Blood to Centenarians. *J Immunol,* 196**,** 5005-13.

CAMAGLIA, F., RYVKIN, A., GREENSTEIN, E., REICH-ZELIGER, S., CHAIN, B., MORA, T., WALCZAK, A. M. & FRIEDMAN, N. 2023. Quantifying changes in the T cell receptor repertoire during thymic development. *Elife,* 12.

CARICO, Z. & KRANGEL, M. S. 2015. Chromatin Dynamics and the Development of the TCRalpha and TCRdelta Repertoires. *Adv Immunol,* 128**,** 307-61.

CARICO, Z. M., ROY CHOUDHURY, K., ZHANG, B., ZHUANG, Y. & KRANGEL, M. S. 2017. Tcrd Rearrangement Redirects a Processive Tcra Recombination Program to Expand the Tcra Repertoire. *Cell Rep,* 19**,** 2157-2173.

CERIANI, L. & VERME, P. 2012. The origins of the Gini index: extracts from Variabilità e Mutabilità (1912) by Corrado Gini. *The Journal of Economic Inequality,* 10**,** 421-443.

CLAUSET, A., SHALIZI, C. R. & NEWMAN, M. E. J. 2009. Power-law distributions in empirical data. *SIAM Review,* 51**,** 661-703.

DESANTI, G. E., COWAN, J. E., BAIK, S., PARNELL, S. M., WHITE, A. J., PENNINGER, J. M., LANE, P. J., JENKINSON, E. J., JENKINSON, W. E. & ANDERSON, G. 2012. Developmentally regulated availability of RANKL and CD40 ligand reveals distinct mechanisms of fetal and adult cross-talk in the thymus medulla. *J Immunol,* 189**,** 5519-26.

DUTTA, A., ZHAO, B. & LOVE, P. E. 2021. New insights into TCR beta-selection. *Trends Immunol,* 42**,** 735-750.

GENOLET, R., STEVENSON, B. J., FARINELLI, L., OSTERAS, M. & LUESCHER, I. F. 2012. Highly diverse TCRalpha chain repertoire of pre-immune CD8(+) T cells reveals new insights in gene recombination. *EMBO J,* 31**,** 4247-8.

GILLESPIE, C. S. 2015. Fitting Heavy Tailed Distributions: The poweRlaw Package. *Journal of Statistical Software,* 64**,** 1-16.

GLANVILLE, J., HUANG, H., NAU, A., HATTON, O., WAGAR, L. E., RUBELT, F., JI, X., HAN, A., KRAMS, S. M., PETTUS, C., HAAS, N., ARLEHAMN, C. S. L., SETTE, A., BOYD, S. D., SCRIBA, T. J., MARTINEZ, O. M. & DAVIS, M. M. 2017. Identifying specificity groups in the T cell receptor repertoire. *Nature,* 547**,** 94-98.

GORDON, J. & MANLEY, N. R. 2011. Mechanisms of thymus organogenesis and morphogenesis. *Development,* 138**,** 3865-78.

GU, Z., EILS, R. & SCHLESNER, M. 2016. Complex heatmaps reveal patterns and correlations in multidimensional genomic data. *Bioinformatics,* 32**,** 2847-2849.

HAGER-THEODORIDES, A. L., ROWBOTHAM, N. J., OUTRAM, S. V., DESSENS, J. T. & CROMPTON, T. 2007. Beta-selection: abundance of TCRbeta-/gammadelta- CD44-CD25- (DN4) cells in the foetal thymus. *Eur J Immunol,* 37**,** 487-500.

JACCARD, P. 1912. The Distribution of the Flora in the Alpine Zone. *The New Phytologist,* 11**,** 37-50.

JOSHI, K., DE MASSY, M. R., ISMAIL, M., READING, J. L., UDDIN, I., WOOLSTON, A., HATIPOGLU, E., OAKES, T., ROSENTHAL, R., PEACOCK, T., RONEL, T., NOURSADEGHI, M., TURATI, V., FURNESS, A. J. S., GEORGIOU, A., WONG, Y. N. S., BEN AISSA, A., SUNDERLAND, M. W., JAMAL-HANJANI, M., VEERIAH, S., BIRKBAK, N. J., WILSON, G. A., HILEY, C. T., GHORANI, E., GUERRA-ASSUNÇÃO, J. A., HERRERO, J., ENVER, T., HADRUP, S. R., HACKSHAW, A., PEGGS, K. S., MCGRANAHAN, N., SWANTON, C., SWANTON, C., JAMAL-HANJANI, M., GEORGIOU, A., SUNDERLAND, M. W., READING, J. L., PEGGS, K. S., GHORANI, E., DE MASSY, M. R., HATIPOGLU, E., QUEZADA, S. A., CHAIN, B., MCGRANAHAN, N., HACKSHAW, A., HILEY, C. T., VEERIAH, S., ROSENTHAL, R., WILSON, G. A., HERRERO, J., BIRKBAK, N. J., NGAI, Y., SHARP, A., RODRIGUES, C., PRESSEY, O., SMITH, S., GOWER, N., DHANDA, H., WATKINS, T. B. K., ESCUDERO, M., STEWART, A., ROWAN, A., GOLDMAN, J., VAN LOO, P., STONE, R. K., DENNER, T., NYE, E., WARD, S., LIM, E., BOEING, S., GRECO, M., BAKIR, M. A., LITCHFIELD, K., NICOD, J., PUTTICK, C., ENFIELD, K., COLLIVER, E., CAMPBELL, B., ABBOSH, C., WU, Y., SKRZYPSKI, M., HYNDS, R. E., MARAFIOTI, T., HARTLEY, J. A., GORMAN, P., LOWE, H. L., ENSELL, L., SPANSWICK, V., KARAMANI, A., MOORE, D., BISWAS, D., RAZAQ, M., BECK, S., HUEBNER, A., DIETZEN, M., NACEUR-LOMBARDELLI, C., AKTHER, M. A., ZHAI, H., KANNU, N., MANZANO, E., et al. 2019. Spatial heterogeneity of the T cell receptor repertoire reflects the mutational landscape in lung cancer. *Nature Medicine,* 25**,** 1549-1559.

KASSAMBARA, A. 2023a. ggpubr: 'ggplot2' Based Publication Ready Plots.

KASSAMBARA, A. 2023b. rstatix: Pipe-Friendly Framework for Basic Statistical Tests. R package version 0.7.2 ed.

KASSAMBARA A, M. F. 2020. factoextra: Extract and Visualize the Results of Multivariate Data Analyses. R package version 1.0.7 ed.

KOLDE, R. 2019. pheatmap: Pretty Heatmaps. R package version 1.0.12 ed.

KONDO, K., OHIGASHI, I. & TAKAHAMA, Y. 2019. Thymus machinery for T-cell selection. *Int Immunol,* 31**,** 119-125.

MONTECINO-RODRIGUEZ, E. & DORSHKIND, K. 2023. The layered development of mouse B and T Cells. *Immunol Rev,* 315**,** 79-88.

OAKES, T., HEATHER, J. M., BEST, K., BYNG-MADDICK, R., HUSOVSKY, C., ISMAIL, M., JOSHI, K., MAXWELL, G., NOURSADEGHI, M., RIDDELL, N., RUEHL, T., TURNER, C. T., UDDIN, I. & CHAIN, B. 2017. Quantitative Characterization of the T Cell Receptor Repertoire of Naive and Memory Subsets Using an Integrated Experimental and Computational Pipeline Which Is Robust, Economical, and Versatile. *Front Immunol,* 8**,** 1267.

OKSANEN, J., BLANCHET, F. G., FRIENDLY, M., KINDT, R., LEGENDRE, P., MCGLINN, D., MINCHIN, P. R., O'HARA, R. B., SIMPSON, G. L., SOLYMOS, P., STEVENS, M. H. H., SZOECS, E. & WAGNER, H. 2022. vegan: Community Ecology Package. R package version 2.6-4 ed.

OUTRAM, S. V., HAGER-THEODORIDES, A. L., SHAH, D. K., ROWBOTHAM, N. J., DRAKOPOULOU, E., ROSS, S. E., LANSKE, B., DESSENS, J. T. & CROMPTON, T. 2009. Indian hedgehog (Ihh) both promotes and restricts thymocyte differentiation. *Blood,* 113**,** 2217-2228.

PARK, J. E., BOTTING, R. A., DOMINGUEZ CONDE, C., POPESCU, D. M., LAVAERT, M., KUNZ, D. J., GOH, I., STEPHENSON, E., RAGAZZINI, R., TUCK, E., WILBREY-CLARK, A., ROBERTS, K., KEDLIAN, V. R., FERDINAND, J. R., HE, X., WEBB, S., MAUNDER, D., VANDAMME, N., MAHBUBANI, K. T., POLANSKI, K., MAMANOVA, L., BOLT, L., CROSSLAND, D., DE RITA, F., FULLER, A., FILBY, A., REYNOLDS, G., DIXON, D., SAEB-PARSY, K., LISGO, S., HENDERSON, D., VENTO-TORMO, R., BAYRAKTAR, O. A., BARKER, R. A., MEYER, K. B., SAEYS, Y., BONFANTI, P., BEHJATI, S., CLATWORTHY, M. R., TAGHON, T., HANIFFA, M. & TEICHMANN, S. A. 2020. A cell atlas of human thymic development defines T cell repertoire formation. *Science,* 367.

POGORELYY, M. V., ELHANATI, Y., MARCOU, Q., SYCHEVA, A. L., KOMECH, E. A., NAZAROV, V. I., BRITANOVA, O. V., CHUDAKOV, D. M., MAMEDOV, I. Z., LEBEDEV, Y. B., MORA, T. & WALCZAK, A. M. 2017. Persisting fetal clonotypes influence the structure and overlap of adult human T cell receptor repertoires. *PLoS Comput Biol,* 13**,** e1005572.

RACKAITYTE, E. & HALKIAS, J. 2020. Mechanisms of Fetal T Cell Tolerance and Immune Regulation. *Front Immunol,* 11**,** 588.

RAMOND, C., BERTHAULT, C., BURLEN-DEFRANOUX, O., DE SOUSA, A. P., GUY-GRAND, D., VIEIRA, P., PEREIRA, P. & CUMANO, A. 2014. Two waves of distinct hematopoietic progenitor cells colonize the fetal thymus. *Nat Immunol,* 15**,** 27-35.

ROSS, J. O., MELICHAR, H. J., AU-YEUNG, B. B., HERZMARK, P., WEISS, A. & ROBEY, E. A. 2014. Distinct phases in the positive selection of CD8+ T cells distinguished by intrathymic migration and T-cell receptor signaling patterns. *Proc Natl Acad Sci U S A,* 111**,** E2550-8.

SCHATZ, D. G. & SWANSON, P. C. 2011. V(D)J recombination: mechanisms of initiation. *Annu Rev Genet,* 45**,** 167-202.

SETHNA, Z., ELHANATI, Y., DUDGEON, C. S., CALLAN, C. G., JR., LEVINE, A. J., MORA, T. & WALCZAK, A. M. 2017. Insights into immune system development and function from mouse T-cell repertoires. *Proc Natl Acad Sci U S A,* 114**,** 2253-2258.

SHANNON, C. E. & WEAVER, W. 1949. *The mathematical theory of communication,* Champaign, IL, US, University of Illinois Press.

SIM, B. C., ZERVA, L., GREENE, M. I. & GASCOIGNE, N. R. 1996. Control of MHC restriction by TCR Valpha CDR1 and CDR2. *Science,* 273**,** 963-6.

SKOK, J. A., GISLER, R., NOVATCHKOVA, M., FARMER, D., DE LAAT, W. & BUSSLINGER, M. 2007. Reversible contraction by looping of the Tcra and Tcrb loci in rearranging thymocytes. *Nat Immunol,* 8**,** 378-87.

SMITH, N. L., PATEL, R. K., REYNALDI, A., GRENIER, J. K., WANG, J., WATSON, N. B., NZINGHA, K., YEE MON, K. J., PENG, S. A., GRIMSON, A., DAVENPORT, M. P. & RUDD, B. D. 2018. Developmental Origin Governs CD8(+) T Cell Fate Decisions during Infection. *Cell,* 174**,** 117-130 e14.

SOLANKI, A., YANEZ, D. C., LAU, C. I., ROWELL, J., BARBARULO, A., ROSS, S., SAHNI, H. & CROMPTON, T. 2020. The transcriptional repressor Bcl6 promotes pre-TCR-induced thymocyte differentiation and attenuates Notch1 activation. *Development,* 147.

SOLANKI, A., YANEZ, D. C., ROSS, S., LAU, C.-I., PAPAIOANNOU, E., LI, J., SALDAÑA, J. I. & CROMPTON, T. 2018. Gli3 in fetal thymic epithelial cells promotes thymocyte positive selection and differentiation by repression of Shh. *Development,* 145.

SUO, C., POLANSKI, K., DANN, E., LINDEBOOM, R. G. H., VILARRASA-BLASI, R., VENTO-TORMO, R., HANIFFA, M., MEYER, K. B., DRATVA, L. M., TUONG, Z. K., CLATWORTHY, M. R. & TEICHMANN, S. A. 2023. Dandelion uses the single-cell adaptive immune receptor repertoire to explore lymphocyte developmental origins. *Nat Biotechnol*.

TEAM, I. 2019. immunarch: An R Package for Painless Bioinformatics Analysis of T-Cell and B-Cell Immune Repertoires.

THOMAS, N., BEST, K., CINELLI, M., REICH-ZELIGER, S., GAL, H., SHIFRUT, E., MADI, A., FRIEDMAN, N., SHAWE-TAYLOR, J. & CHAIN, B. 2014. Tracking global changes induced in the CD4 T-cell receptor repertoire by immunization with a complex antigen using short stretches of CDR3 protein sequence. *Bioinformatics,* 30**,** 3181-3188.

THOMAS, N., HEATHER, J., NDIFON, W., SHAWE-TAYLOR, J. & CHAIN, B. 2013. Decombinator: a tool for fast, efficient gene assignment in T-cell receptor sequences using a finite state machine. *Bioinformatics,* 29**,** 542-550.

UDDIN, I., JOSHI, K., OAKES, T., HEATHER, J. M., SWANTON, C., CONSORTIUM, T. R. & CHAIN, B. 2019. An Economical, Quantitative, and Robust Protocol for High-Throughput T Cell Receptor Sequencing from Tumor or Blood. *Methods Mol Biol,* 1884**,** 15-42.

WANG, J., WISSINK, E. M., WATSON, N. B., SMITH, N. L., GRIMSON, A. & RUDD, B. D. 2016. Fetal and adult progenitors give rise to unique populations of CD8+ T cells. *Blood,* 128**,** 3073-3082.

WICKHAM, H. 2016. *ggplot2: Elegant Graphics for Data Analysis*, Springer-Verlag New York.

WICKHAM H, A. M., BRYAN J, CHANG W, MCGOWAN LD, FRANÇOIS R, GROLEMUND G, HAYES A, HENRY L, HESTER J, KUHN M, PEDERSEN TL, MILLER E, BACHE SM, MÜLLER K, OOMS J, ROBINSON D, SEIDEL DP, SPINU V, TAKAHASHI K, VAUGHAN D, WILKE C, WOO K, YUTANI H 2019. Welcome to the tidyverse. *Journal of Open Source Software,* 4**,** 1686.

WONG, W. K., LEEM, J. & DEANE, C. M. 2019. Comparative Analysis of the CDR Loops of Antigen Receptors. *Front Immunol,* 10**,** 2454.

XIAO, S. Y., LI, Y. & CHEN, W. F. 2003. Kinetics of thymocyte developmental process in fetal and neonatal mice. *Cell Res,* 13**,** 265-73.

ZEILEIS, A. 2014. ineq: Measuring Inequality, Concentration, and Poverty. R package version 0.2-13 ed.

Figure Legends

Figure 1. Decreased diversity and increased clonality of foetal compared to young adult TCRβ repertoires

TCR β-chain repertoires were sequenced from FACS-sorted $CD4^+CD8^+$ (DP), $CD4^+CD8^-CD3^+$ (SP4) and $CD4^-CD8^+CD3^+$ (SP8) thymocyte populations from E18.5 (red circles; n=4) and 4 week-old (blue circles; n=4) C57BL/6 thymus.

(A) The frequency distribution of TCR β-chain abundance was fitted to a discrete power law ($f(k) = Ck^{-\alpha}$) by maximum likelihood (solid line). These logged plots show the mean frequency distribution for E18.5 and 4 weeks in DP, SP4 and SP8 populations. The *x* axis represents TCR abundance (size of clone), and the *y* axis represents the proportion of the repertoire. The negative of the power law exponent corresponds to the slope of the logged plot. Each point represents a mean from four mice/embryos. **(B)** The power law exponents of the frequency distribution of TCR β-chain abundances for E18.5 and 4 weeks in DP, SP4 and SP8 populations, where each point represents an individual mouse/embryo. **(C)** The proportion of the total TCR β-chain repertoire accounted for by the expanded top 1% most abundant sequences (>99th percentile) for E18.5 and 4 weeks for DP, SP4 and SP8 populations, where each point represents an individual mouse/embryo. **(D)** The number of β-chain sequences detected above the given frequency threshold (top 1% most abundant sequences) is shown for E18.5 (red circles) and 4 weeks (blue circles) in DP, SP4 and SP8 populations. Each small translucent point represents the abundance of any β-chain sequence detected above the threshold for all mice/embryos at that life-stage, while each larger solid point represents the mean of β-chain sequence abundance for each individual mouse/embryo. (**E)** The Shannon entropies for the β-chain TCR repertoires of E18.5 and 4 weeks in DP populations, where each point represents an individual mouse/embryo. Each repertoire was subsampled to 25000 TCRs 1000 times before calculating the Shannon entropy. **(F)** The Shannon entropies for the β-chain TCR repertoires of E18.5 and 4 weeks in SP4 and SP8 populations, where each point represents an individual mouse/embryo. Each repertoire was subsampled to 750 TCRs

1000 times before calculating the Shannon entropy. **(G)** The Gini indexes for the β-chain TCR repertoires of E18.5 and 4 weeks in DP populations, where each point represents an individual mouse/embryo. Each repertoire was subsampled to 25000 TCRs 1000 times before calculating the Gini index. **(H)** The Gini indexes for the β-chain TCR repertoires of E18.5 and 4 weeks in SP4 and SP8 populations, where each point represents an individual mouse/embryo. Each repertoire was subsampled to 750 TCRs 1000 times before calculating the Gini index. Dotplots show mean±c.i and statistical comparisons were carried out by unpaired Student's t-test or Welch's t-test as appropriate: *** p <0.001; ** p <0.01; *p < 0.05.

Figure 2. Foetal and young adult TCR repertoires favour different gene segments

TCR α-chain (A-B) and β-chain (C-G) repertoires were sequenced from FACS-sorted $CD4^+CD8^-CD3^+$ (SP4) and $CD4^-CD8^+CD3^+$ (SP8) $CD4^+CD8^+CD69^-$ (CD69-DP, foetal), $CD4^+CD8^+CD69^+$ ($CD69^+$DP foetal) $CD4^+CD8^+CD3^{-/lo}$ ($CD3^{-/lo}$DP, adult), $CD4^+CD8^+CD3^{+/hi}$ ($CD3^{+/hi}$DP adult) thymocyte populations from E18.5 (red; n=4) and 4 week-old (blue; n=4) C57BL/6 thymus. DP, SP4 and SP8 populations are coloured in green, orange and purple respectively.

(A-D) Heatmaps of proportional α-chain variable (V) **(A)**, α-chain joining (J) **(B),** β-chain V**(C)** and β-chain J **(D)** gene usage of unique TCRs for E18.5 and 4 weeks in DP, SP4 and SP8 populations. Each column represents a mean of 4 embryos or mice and was clustered using Euclidian distance. Genes are shown in chromosomal order (5' to 3') from top to bottom. **(E-G)** PCA biplot of β-chain V and J gene counts of unique TCRs for E18.5 and 4 weeks in DP, **(E)** SP4 **(F)** and SP8 **(G)** populations.

Figure 3. Principal Component Analysis (PCA) of Variable x Joining combinations in embryonic and young adult TCRβ repertoires cluster by life-stage before cell-type

TCR β-chain repertoires were sequenced from FACS-sorted $CD4^+CD8^+$ (DP), $CD4^+CD8^-CD3^+$ (SP4) and $CD4^-CD8^+CD3^+$ (SP8) thymocyte populations from E18.5 (n=4) and 4 week-old (n=4) C57BL/6 thymus.

(A-B) PCA biplot of β-chain VxJ gene counts of unique TCRβ sequences for E18.5 and 4 weeks in DP, SP4 and SP8 populations. **(A)** E18.5 and 4 weeks are coloured in red and blue circles respectively. **(B)** DP, SP4 and SP8 populations are coloured in green, orange and purple respectively. **(C)** Top 10 highest β-chain VxJ gene combinations that contribute to PC1 and PC2 of the PCA.

Figure 4. Different VxJ combinations in foetal and young adult repertoires by cell-type

TCR β-chain and α-chain repertoires were sequenced from FACS-sorted $CD4^+CD8^+$ (DP), $CD4^+CD8^-CD3^+$ (SP4) and $CD4^-CD8^+CD3^+$ (SP8) thymocyte populations from E18.5 (red; n=4) and 4 week-old (blue; n=4) C57BL/6 thymus.

(A-C) Plots show β-chain (left column) and α-chain (right column) proportional VxJ gene usage of total TCRs for E18.5 compared to 4 weeks in DP **(A)**, SP4 **(B)** and SP8 **(C)** populations. Red tiles signify increased usage of VxJ combinations in E18.5 ($p < 0.05$), while blue tiles signify decreased usage in E18.5 ($p < 0.05$) compared to 4 weeks. Light grey tiles signify no change in gene usage ($p > 0.05$), yellow tiles signify VxJ combinations not detected in E18.5, brown tiles signify VxJ combinations not detected in 4 weeks and black tiles signify VxJ combinations not detected in both E18.5 and 4 weeks. Only combinations that were detected in all 8 mice/embryos were compared. Dark grey tiles signify combinations that were not compared. Statistical comparisons were carried out by unpaired Student's t-test followed by FDR-adjustment (5%, Benjamini-Hochberg procedure) of *p* values.

Figure 5. Decreased TCRβ non-template insertions, CDR3 length and increased CDR3 sharing in foetal compared to young adult

TCR β-chain repertoires were sequenced from FACS-sorted $CD4^+CD8^+$ (DP), $CD4^+CD8^-CD3^+$ (SP4) and $CD4^-CD8^+CD3^+$ (SP8) thymocyte populations from E18.5 (red circles; n=4) and 4 week-old (blue circles; n=4) C57BL/6 thymus.

(A) Percentage of non-productive β-chain TCRs from total rearrangements for E18.5 and 4 weeks in DP, SP4 and SP8 populations. **(B)** The weighted mean of non-template insertion length for all β -chain TCRs (basepairs) for E18.5 and 4 weeks in DP, SP4 and SP8 populations. **(C)** The mean of β-chain unique predicted CDR3 length (number of amino acids) for E18.5 and 4 weeks in DP, SP4 and SP8 populations. **(D)** The intra life-stage Jaccard Index of Similarity of β-chain CDR3s for E18.5 and 4 weeks in the DP population. Each repertoire was subsampled to 17000 CDR3s 1000 times before calculating the Jaccard Index. **(E)** The intra life-stage Jaccard Index of Similarity of β-chain CDR3s for E18.5 and 4 weeks in the SP4 and SP8 population. Each repertoire was subsampled to 700 CDR3s 1000 times before calculating the Jaccard Index. **(F)** The intra life-stage Jaccard Index of Similarity of sequential β-chain CDR3 amino acid triplets (k-mers) for E18.5 and 4 weeks in the DP population. Each repertoire was subsampled to 100000 k-mers 1000 times before calculating the Jaccard Index. **(G)** The intra life-stage Jaccard Index of Similarity of sequential β-chain CDR3 amino acid triplets for E18.5 and 4 weeks in the SP4 and SP8 population. Each repertoire was subsampled to 5000 k-mers 1000 times before calculating the Jaccard Index. **(H-I)** PCA biplot of β-chain CDR3 amino acid triplet frequency distributions for E18.5 and 4 weeks in DP, SP4 and SP8 population. **(H)** E18.5 and 4-week samples are coloured in red and blue respectively, while in **(I)** DP, SP4 and SP8 populations are coloured green, orange and purple respectively. Dotplots show mean±c.i and statistical comparisons were carried out by unpaired Student's t-test or Welch's t-test as appropriate: *** p <0.001; ** p <0.01; *p < 0.05.

Figure 6. Differences in CDR1xCDR2 combinations in foetal and young adult thymocyte populations

TCR β-chain and α-chain repertoires were sequenced from FACS-sorted $CD4^+CD8^+$ (DP), $CD4^+CD8^-CD3^+$ (SP4) and $CD4^-CD8^+CD3^+$ (SP8) thymocyte populations from E18.5 (n=4) and 4-week-old (n=4) C57BL/6 thymus and frequency of CDR1 and CDR2 sequences calculated for

each population. E18.5 and 4-week samples are coloured red and blue respectively, while DP, SP4 and SP8 populations are coloured green, orange and purple respectively.

(A-B) PCA biplot of β-chain CDR1xCDR2 frequency distributions for E18.5 and 4 weeks in DP, SP4 and SP8 populations. In **(A),** E18.5 and 4-weeks samples are coloured in red and blue respectively, while in **(B)**, DP, SP4 and SP8 populations are coloured in green, orange and purple respectively. **(C)** Top 10 highest CDR1xCDR2 combinations that contribute to PC1 and PC2 of the PCA of β-chain CDR1xCDR2 frequency distributions for E18.5 and 4 weeks in DP, SP4 and SP8 population (shown in A-B). **(D)** Heatmap of proportional β-chain CDR1xCDR2 usage E18.5 and 4 weeks in DP, SP4 and SP8 populations. Each column represents a mean of 4 embryos or mice and was clustered using Euclidian distance, while rows (CDR1 x CDR2 combinations) were clustered using Pearson correlation. **(E)** Heatmap of proportional α-chain CDR1xCDR2 usage in E18.5 and 4 week samples in DP, SP4 and SP8 populations. Each column represents a mean of 4 embryos or mice and was clustered using Euclidian distance, while rows (CDR1xCDR2 combinations) were clustered using Pearson correlation.

Figure 7. Hydrocortisone-treated young adult DP gene segment usage becomes more foetal like

TCR α-chain (A-C) and β-chain (D-F) repertoires were sequenced from FACS-sorted $CD4^{+}CD8^{+}CD69^{-}$ (CD69-DP, foetal), $CD4^{+}CD8^{+}CD69^{+}$ ($CD69^{+}$DP foetal) $CD4^{+}CD8^{+}CD3^{-/lo}$ ($CD3^{-/lo}$DP, adult), $CD4^{+}CD8^{+}CD3^{+/hi}$ ($CD3^{+/hi}$DP adult) thymocyte populations from E18.5 (red; n=4), 4 week-old (blue; n=4), and 4 week-old treated with hydrocortisone on day 6 after treatment (light blue; n=5) C57BL/6 thymus.

(A-B) Heatmaps of proportional α-chain variable (V) **(A)** and α-chain joining (J) **(B)** gene usage of unique TCRs for E18.5, 4 weeks (control) and 4 weeks treated with hydrocortisone in DP populations. Each column represents a mean of 4 (E18.5 and 4 weeks) or 5 (4 weeks treated with hydrocortisone) embryos or mice and was clustered using Euclidian distance. Genes are shown in chromosomal order (5' to 3') from top to bottom. **(C)** Plot shows α-chain

proportional VxJ gene usage of total TCRs for 4 weeks HC-treated compared to 4 weeks (control) in DP populations. Pink tiles signify increased usage of VxJ combinations in 4 weeks HC-treated ($p < 0.05$), while green tiles signify decreased usage in 4 weeks HC-treated ($p < 0.05$) compared to 4 weeks (control). Grey tiles signify no change in gene usage ($p > 0.05$), yellow tiles signify VxJ combinations not detected in 4 weeks HC-treated, brown tiles signify VxJ combinations not detected in 4 weeks (control) and black tiles signify VxJ combinations not detected in both 4 weeks HC-treated and 4 weeks (control). Only combinations that were detected in all 9 mice were compared. Dark grey tiles signify combinations that were not compared. Statistical comparisons were carried out by unpaired Student's t-test followed by FDR-adjustment (5%, Benjamini-Hochberg procedure) of *p* values. **(D-E)** Heatmaps of proportional β-chain V**(D)** and β-chain J **(E)** gene usage of unique TCRs for E18.5, 4 weeks (control) and 4 weeks treated with hydrocortisone in DP populations. Each column represents a mean of 4 (E18.5 and 4 weeks) or 5 (4 weeks treated with hydrocortisone) embryos or mice and was clustered using Euclidian distance. Genes are shown in chromosomal order (5' to 3') from top to bottom. **(F)** Plot shows β-chain proportional VxJ gene usage of total TCRs for 4 weeks HC-treated compared to 4 weeks (control) in DP populations. Pink tiles signify increased usage of VxJ combinations in 4 weeks HC-treated ($p < 0.05$), while green tiles signify decreased usage in 4 weeks HC-treated ($p < 0.05$) compared to 4 weeks (control). Grey tiles signify no significant change in gene usage ($p > 0.05$), yellow tiles signify VxJ combinations not detected in 4 weeks HC-treated, brown tiles signify VxJ combinations not detected in 4 weeks (control) and black tiles signify VxJ combinations not detected in both 4 weeks HC-treated and 4 weeks (control). Statistical comparisons were carried out by unpaired Student's t-test followed by FDR-adjustment (5%, Benjamini-Hochberg procedure) of *p* values.

Supplementary Figure Legends

Supplementary Figure 1: Distribution and diversity of embryonic and young adult TCRα repertoire

TCR α-chain repertoires were sequenced from FACS-sorted $CD4^+CD8^+$ (DP), $CD4^+CD8^-CD3^+$ (SP4) and $CD4^-CD8^+CD3^+$ (SP8) thymocyte populations from E18.5 (red circles; n=4) and 4 week-old (blue circles; n=4) C57BL/6 thymus.

(A) The frequency distribution of TCR α-chain abundance was fitted to a discrete power law ($f(k) = Ck^{-\alpha}$) by maximum likelihood. These logged plots show the mean frequency distribution for E18.5 and 4 weeks in DP, SP4 and SP8 populations. The *x* axis represents TCR abundance (size of clone), and the *y* axis represents the proportion of the repertoire. The negative of the power law exponent corresponds to the slope of the logged plot. Each point represents a mean from four mice/embryos. **(B)** The power law exponents of the frequency distribution of TCR α-chain abundances for E18.5 and 4 weeks in DP, SP4 and SP8 populations, where each point represents an individual mouse/embryo. **(C)** The proportion of the total TCR α-chain repertoire accounted for by the expanded top 1% most abundant sequences (>99th percentile) for E18.5 and 4 weeks for DP, SP4 and SP8 populations, where each point represents an individual mouse/embryo. **(D)** The number of α-chain sequences detected above the given frequency threshold (top 1% most abundant sequences) is shown for E18.5 (red circles) and 4 weeks (blue circles) in DP, SP4 and SP8 populations. Each small translucent point represents the abundance of any β-chain sequence detected above the threshold for all mice/embryos at that life-stage, while each larger solid point represents the mean of α-chain sequence abundance for each individual mouse/embryo. (**E)** The Shannon entropies for the α-chain TCR repertoires of E18.5 and 4 weeks in DP populations, where each point represents an individual mouse/embryo. Each repertoire was subsampled to 25000 TCRs 1000 times before calculating the Shannon entropy. **(F)** The Shannon entropies for the α-chain TCR repertoires of E18.5 and 4 weeks in SP4 and SP8 populations, where each point represents an individual mouse/embryo. Each repertoire was

subsampled to 750 TCRs 1000 times before calculating the Shannon entropy. **(G)** The Gini indexes for the α-chain TCR repertoires of E18.5 and 4 weeks in DP populations, where each point represents an individual mouse/embryo. Each repertoire was subsampled to 25000 TCRs 1000 times before calculating the Gini index. **(H)** The Gini indexes for the α-chain TCR repertoires of E18.5 and 4 weeks in SP4 and SP8 populations, where each point represents an individual mouse/embryo. Each repertoire was subsampled to 750 TCRs 1000 times before calculating the Gini index.

Dotplots show mean±c.i and statistical comparisons were carried out by unpaired Student's t-test or Welch's t-test as appropriate: *** p <0.001; ** p <0.01; *p < 0.05.

Supplementary Figure 2: Foetal and young adult DP populations have proportionally different TRAV, TRAJ, TRBV and TRBJ gene usage

(A-D) Dotplots show proportional TRAV **(A)**, TRAJ **(B)**, TRBV **(C)**, and TRBJ **(D)** gene usage of unique TCRs for E18.5 (red circles) and 4 weeks (blue circles) in DP populations. Genes are shown in chromosomal order (5' to 3') from left to right. Dots represent individual mice (n=4) and bars show the mean. Statistical comparisons were carried out by unpaired Student's t-test or Welch's t-test as appropriate. Genes significantly increased were highlighted in red (when increased in E18.5) or blue (when increased in 4 weeks). *** p <0.001; ** p <0.01; *p < 0.05.

Supplementary Figure 3: Foetal and young adult SP4 populations have proportionally different TRAV, TRAJ, TRBV and TRBJ gene usage

(A-D) Dotplots show proportional TRAV **(A)**, TRAJ **(B)**, TRBV **(C)**, and TRBJ **(D)** gene usage of unique TCRs for E18.5 (red circles) and 4 weeks (blue circles) in SP4 populations. Genes are shown in chromosomal order (5' to 3') from left to right. Dots represent individual mice (n=4) and bars show the mean. Statistical comparisons were carried out by unpaired Student's t-test or Welch's t-test as appropriate. Genes significantly increased were highlighted in red

(when increased in E18.5) or blue (when increased in 4 weeks). *** p <0.001; ** p <0.01; *p < 0.05.

Supplementary Figure 4: Foetal and young adult SP8 populations have proportionally different TRAV, TRAJ, TRBV and TRBJ gene usage

(A-D) Dotplots show proportional TRAV **(A)**, TRAJ **(B)**, TRBV **(C)**, and TRBJ **(D)** gene usage of unique TCRs for E18.5 (red circles) and 4 weeks (blue circles) in SP8 populations. Genes are shown in chromosomal order (5' to 3') from left to right. Dots represent individual mice (n=4) and bars show the mean. Statistical comparisons were carried out by unpaired Student's t-test or Welch's t-test as appropriate. Genes significantly increased were highlighted in red (when increased in E18.5) or blue (when increased in 4 weeks). *** p <0.001; ** p <0.01; *p < 0.05.

Supplementary Figure 5: Predicted TCRα CDR3 non-template insertions, length and sharing in foetal and young adult thymocyte populations

(A) Percentage of non-productive α-chain TCRs from total rearrangements for E18.5 and 4 weeks in DP, SP4 and SP8 populations. **(B)** The weighted mean of non-template insertion length for all α-chain TCRs (basepairs) for E18.5 and 4 weeks in DP, SP4 and SP8 populations. **(C)** The mean of α-chain unique predicted CDR3 length (number of amino acids) for E18.5 and 4 weeks in DP, SP4 and SP8 populations. **(D)** The intra life-stage Jaccard Index of Similarity of α-chain CDR3s for E18.5 and 4 weeks in the DP population. Each repertoire was subsampled to 17000 CDR3s 1000 times before calculating the Jaccard Index. **(E)** The intra life-stage Jaccard Index of Similarity of α-chain CDR3s for E18.5 and 4 weeks in the SP4 and SP8 population. Each repertoire was subsampled to 700 CDR3s 1000 times before calculating the Jaccard Index. **(F)** The intra life-stage Jaccard Index of Similarity of α-chain CDR3 amino acid triplets (k-mers) for E18.5 and 4 weeks in the DP population. Each repertoire was subsampled to 100000 amino acid triplets 1000 times before calculating the Jaccard Index. **(G)** The intra

life-stage Jaccard Index of Similarity of α-chain CDR3 amino acid triplets (k-mers) for E18.5 and 4-week in the SP4 and SP8 population. Each repertoire was subsampled to 5000 amino acid triplets 1000 times before calculating the Jaccard Index. **(H-I)** PCA biplot of α-chain CDR3 amino acid triplet frequency distributions for E18.5 and 4-week in DP, SP4 and SP8 population. **(H)** E18.5 and 4-week samples are coloured in red and blue respectively, while in **(I)** DP, SP4 and SP8 populations are coloured green, orange and purple respectively.

Dotplots show mean±c.i and statistical comparisons were carried out by unpaired Student's t-test or Welch's t-test as appropriate: *** p <0.001; ** p <0.01; *p < 0.05.

Supplementary Figure 6: PCA of α-chain CDR1xCDR2 frequency distributions in foetal and young adult thymocyte populations

(A-B) PCA biplot of α-chain CDR1xCDR2 frequency distributions for E18.5 and 4-weeks in DP, SP4 and SP8 populations. In (**A),** E18.5 and 4-weeks samples are coloured in red and blue respectively, while in (**B)**, DP, SP4 and SP8 populations are coloured in green, orange and purple respectively.

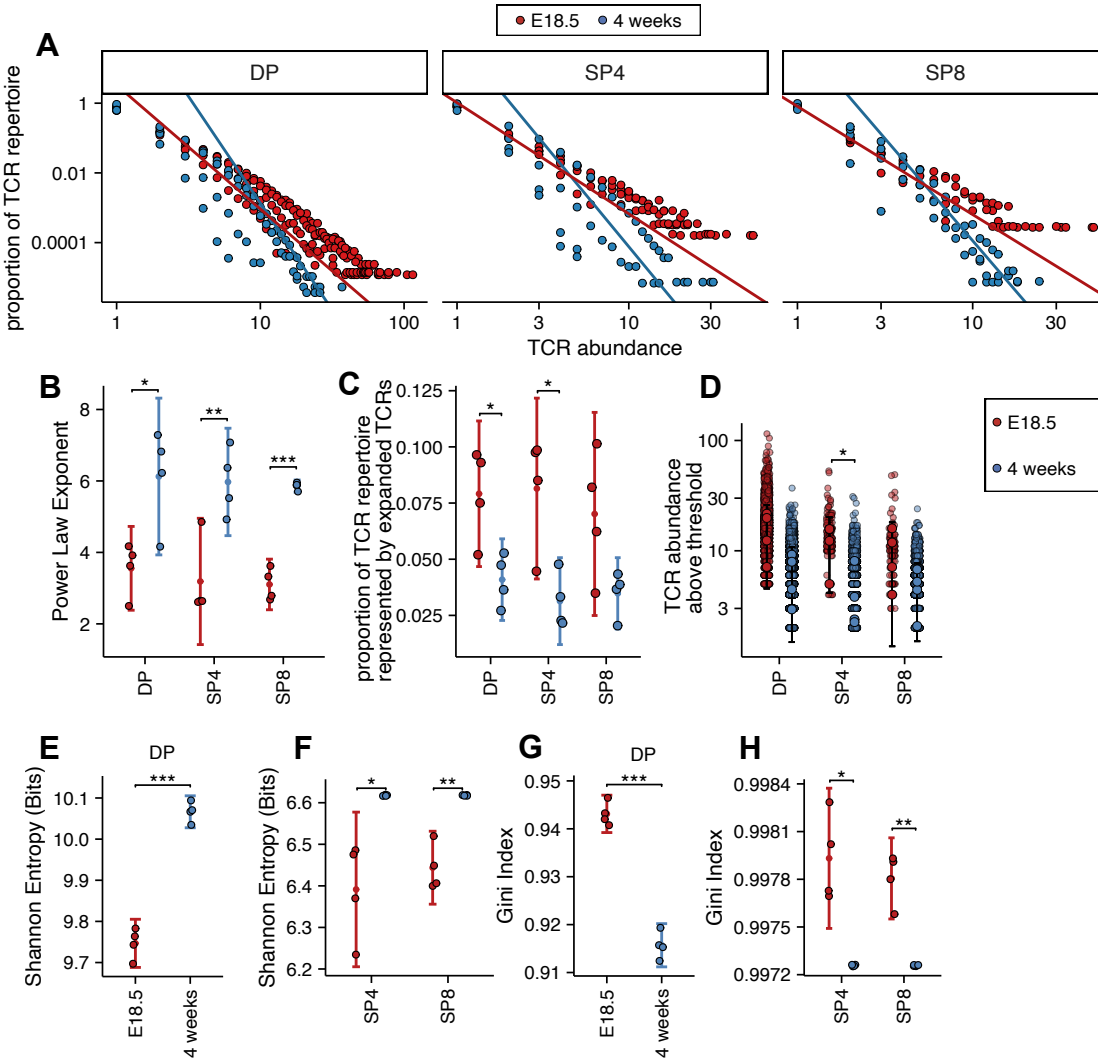
E18.5
4 weeks
A
DP
SP4
SP8
proportion of TCR repertoire
TCR abundance
B
Power Law Exponent
C
proportion of TCR repertoire represented by expanded TCRs
D
TCR abundance above threshold
E
Shannon Entropy (Bits)
F
G
Gini Index
H

Figure 1

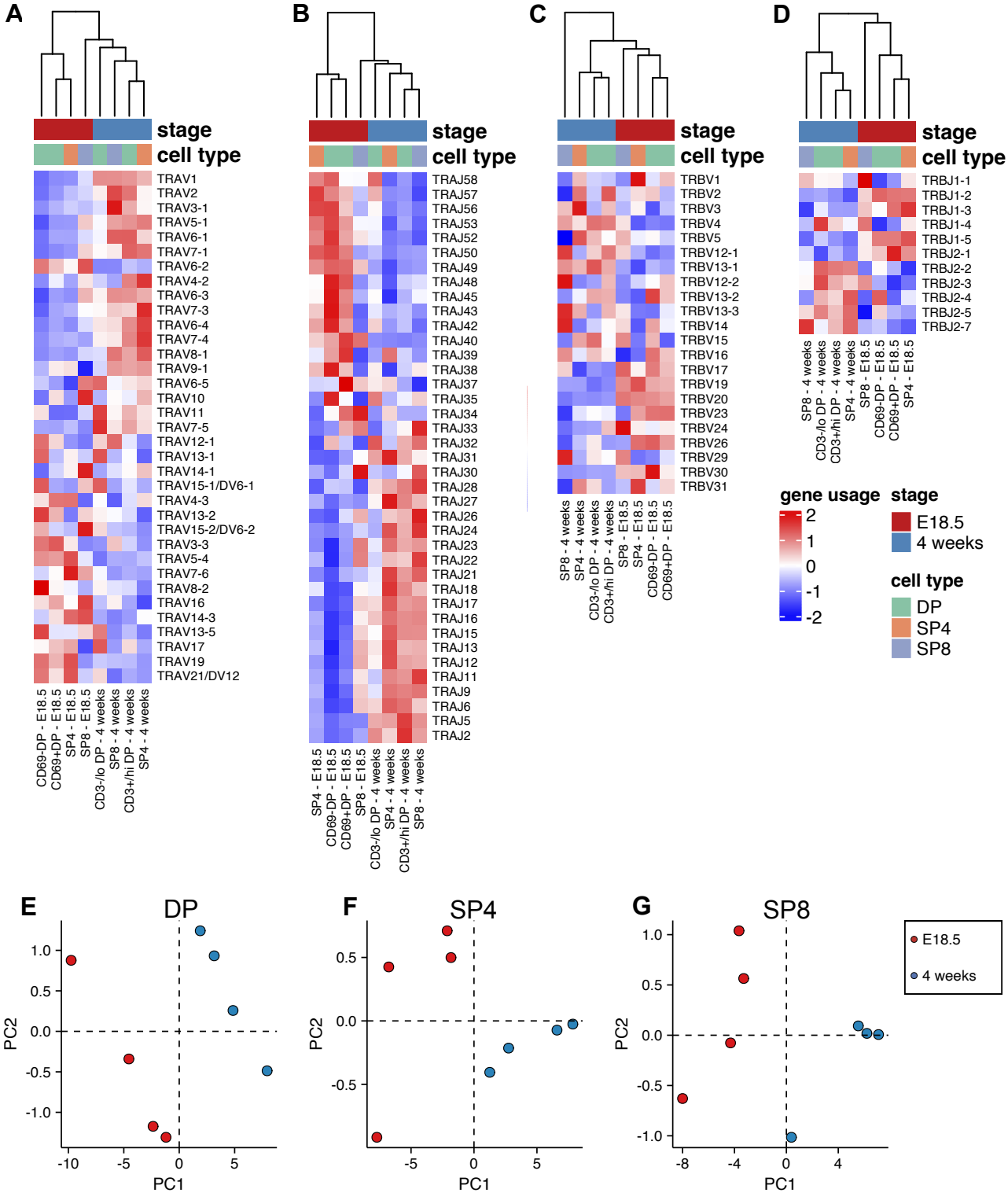
A
B
C
D
stage
cell type
TRAV1
TRAV2
TRAV3-1
TRAV5-1
TRAV6-1
TRAV7-1
TRAV6-2
TRAV4-2
TRAV6-3
TRAV7-3
TRAV6-4
TRAV7-4
TRAV8-1
TRAV9-1
TRAV6-5
TRAV10
TRAV11
TRAV7-5
TRAV12-1
TRAV13-1
TRAV14-1
TRAV15-1/DV6-1
TRAV4-3
TRAV13-2
TRAV15-2/DV6-2
TRAV3-3
TRAV5-4
TRAV7-6
TRAV8-2
TRAV16
TRAV14-3
TRAV13-5
TRAV17
TRAV19
TRAV21/DV12
CD69-DP - E18.5
CD69+DP - E18.5
SP4 - E18.5
SP8 - E18.5
CD3-/lo DP - 4 weeks
SP8 - 4 weeks
CD3+/hi DP - 4 weeks
SP4 - 4 weeks
TRAJ58
TRAJ57
TRAJ56
TRAJ53
TRAJ52
TRAJ50
TRAJ49
TRAJ48
TRAJ45
TRAJ43
TRAJ42
TRAJ40
TRAJ39
TRAJ38
TRAJ37
TRAJ35
TRAJ34
TRAJ33
TRAJ32
TRAJ31
TRAJ30
TRAJ28
TRAJ27
TRAJ26
TRAJ24
TRAJ23
TRAJ22
TRAJ21
TRAJ18
TRAJ17
TRAJ16
TRAJ15
TRAJ13
TRAJ12
TRAJ11
TRAJ9
TRAJ6
TRAJ5
TRAJ2
TRBV1
TRBV2
TRBV3
TRBV4
TRBV5
TRBV12-1
TRBV13-1
TRBV12-2
TRBV13-2
TRBV13-3
TRBV14
TRBV15
TRBV16
TRBV17
TRBV19
TRBV20
TRBV23
TRBV24
TRBV26
TRBV29
TRBV30
TRBV31
SP8 - 4 weeks
SP4 - 4 weeks
CD3-/lo DP - 4 weeks
CD3+/hi DP - 4 weeks
SP8 - E18.5
SP4 - E18.5
CD69-DP - E18.5
CD69+DP - E18.5
TRBJ1-1
TRBJ1-2
TRBJ1-3
TRBJ1-4
TRBJ1-5
TRBJ2-1
TRBJ2-2
TRBJ2-3
TRBJ2-4
TRBJ2-5
TRBJ2-7
gene usage
2
1
0
-1
-2
stage
E18.5
4 weeks
cell type
DP
SP4
SP8
E
DP
F
SP4
G
SP8
PC1
PC2
E18.5
4 weeks

Figure 2

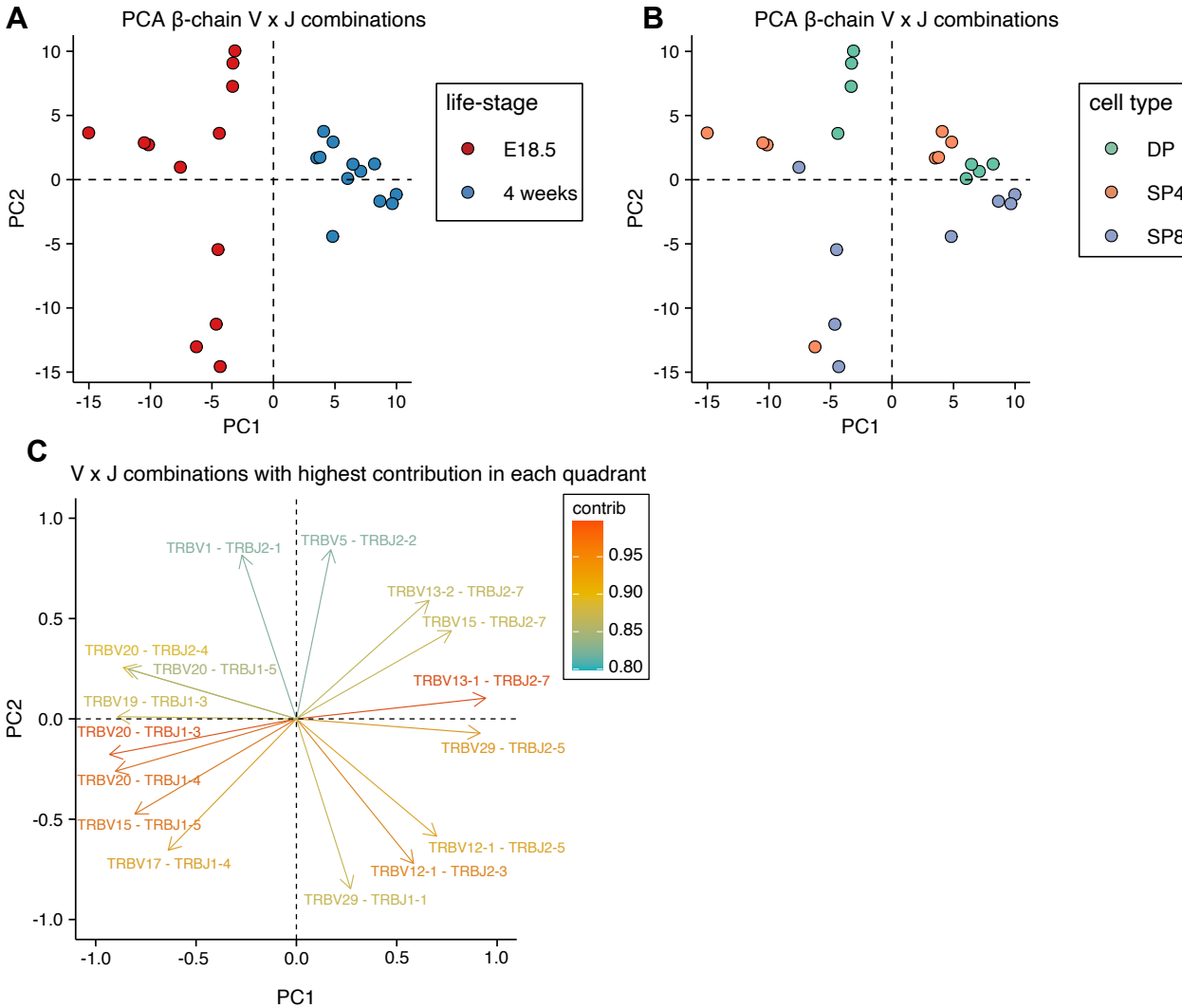
A
PCA β-chain V x J combinations
PC2
PC1
life-stage
E18.5
4 weeks
B
PCA β-chain V x J combinations
PC2
PC1
cell type
DP
SP4
SP8
C
V x J combinations with highest contribution in each quadrant
contrib
0.95
0.90
0.85
0.80
TRBV1 - TRBJ2-1
TRBV5 - TRBJ2-2
TRBV13-2 - TRBJ2-7
TRBV15 - TRBJ2-7
TRBV20 - TRBJ2-4
TRBV20 - TRBJ1-5
TRBV13-1 - TRBJ2-7
TRBV19 - TRBJ1-3
TRBV20 - TRBJ1-3
TRBV29 - TRBJ2-5
TRBV20 - TRBJ1-4
TRBV15 - TRBJ1-5
TRBV12-1 - TRBJ2-5
TRBV17 - TRBJ1-4
TRBV12-1 - TRBJ2-3
TRBV29 - TRBJ1-1
PC2
PC1

Figure 3

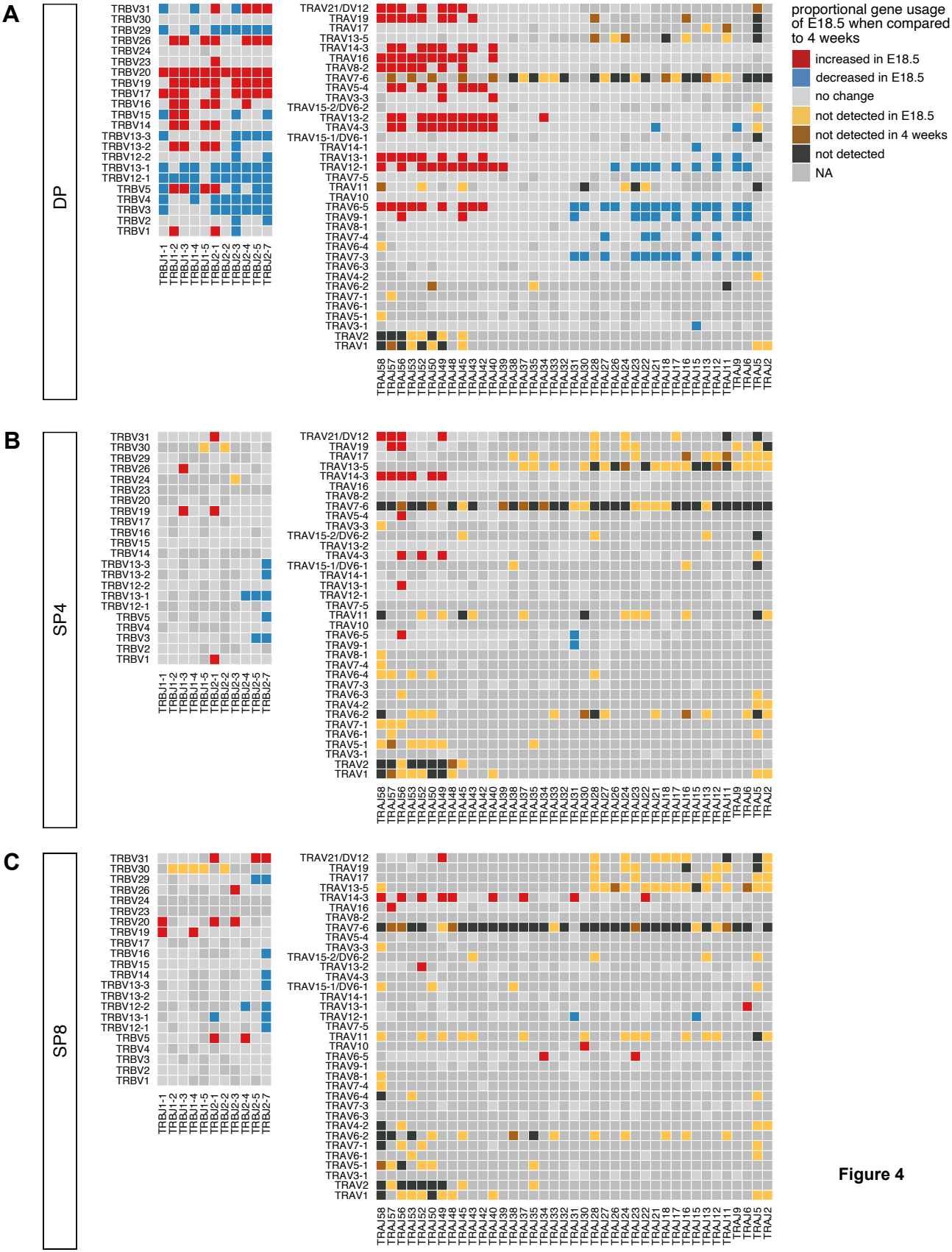
A
DP
B
SP4
C
SP8
TRBV31
TRBV30
TRBV29
TRBV26
TRBV24
TRBV23
TRBV20
TRBV19
TRBV17
TRBV16
TRBV15
TRBV14
TRBV13-3
TRBV13-2
TRBV12-2
TRBV13-1
TRBV12-1
TRBV5
TRBV4
TRBV3
TRBV2
TRBV1
TRBJ1-1
TRBJ1-2
TRBJ1-3
TRBJ1-4
TRBJ1-5
TRBJ2-1
TRBJ2-2
TRBJ2-3
TRBJ2-4
TRBJ2-5
TRBJ2-7
TRAV21/DV12
TRAV19
TRAV17
TRAV13-5
TRAV14-3
TRAV16
TRAV8-2
TRAV7-6
TRAV5-4
TRAV3-3
TRAV15-2/DV6-2
TRAV13-2
TRAV4-3
TRAV15-1/DV6-1
TRAV14-1
TRAV13-1
TRAV12-1
TRAV7-5
TRAV11
TRAV10
TRAV6-5
TRAV9-1
TRAV8-1
TRAV7-4
TRAV6-4
TRAV7-3
TRAV6-3
TRAV4-2
TRAV6-2
TRAV7-1
TRAV6-1
TRAV5-1
TRAV3-1
TRAV2
TRAV1
TRAJ58
TRAJ57
TRAJ56
TRAJ53
TRAJ52
TRAJ50
TRAJ49
TRAJ48
TRAJ45
TRAJ43
TRAJ42
TRAJ40
TRAJ39
TRAJ38
TRAJ37
TRAJ35
TRAJ34
TRAJ33
TRAJ32
TRAJ31
TRAJ30
TRAJ28
TRAJ27
TRAJ26
TRAJ24
TRAJ23
TRAJ22
TRAJ21
TRAJ18
TRAJ17
TRAJ16
TRAJ15
TRAJ13
TRAJ12
TRAJ11
TRAJ9
TRAJ6
TRAJ5
TRAJ2
proportional gene usage of E18.5 when compared to 4 weeks
increased in E18.5
decreased in E18.5
no change
not detected in E18.5
not detected in 4 weeks
not detected
NA

Figure 4

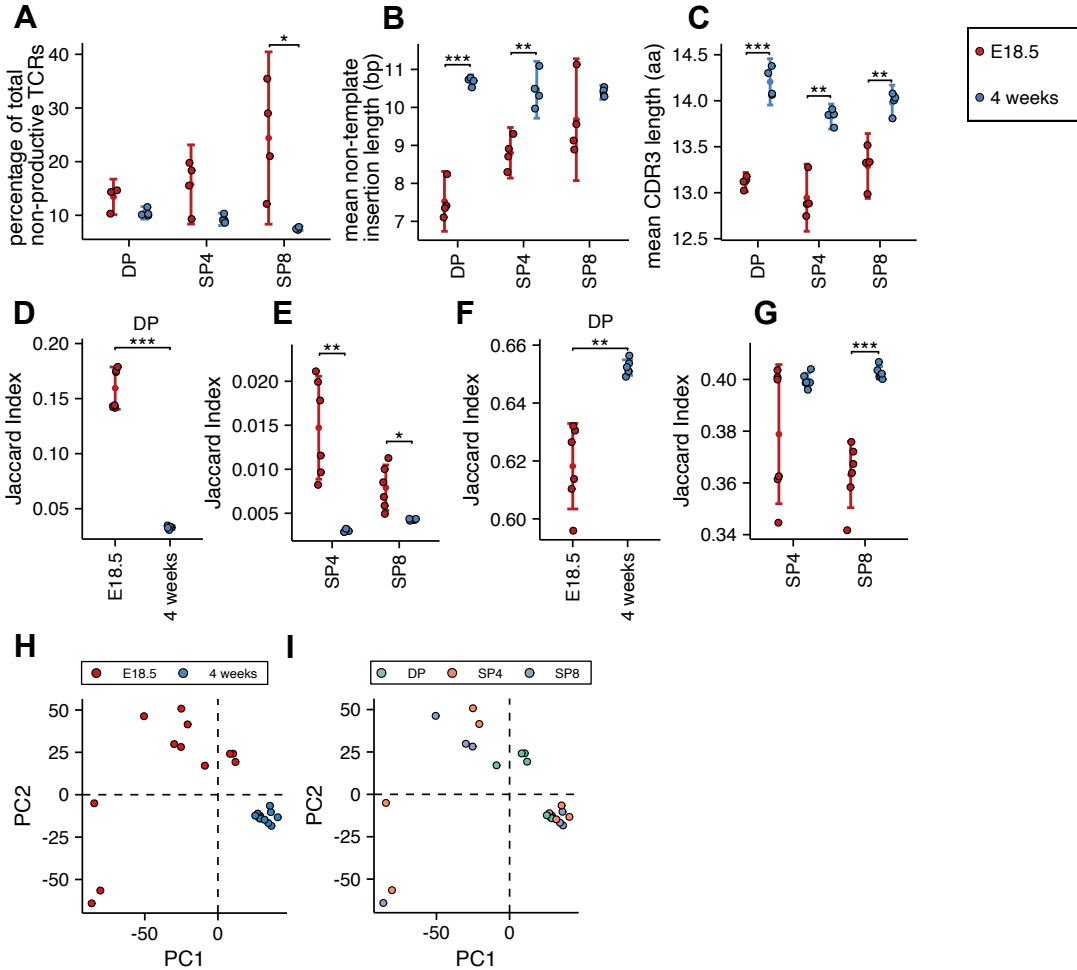
A
percentage of total non-productive TCRs
DP
SP4
SP8
B
mean non-template insertion length (bp)
C
mean CDR3 length (aa)
E18.5
4 weeks
D
Jaccard Index
E
F
G
H
PC1
PC2
I

Figure 5

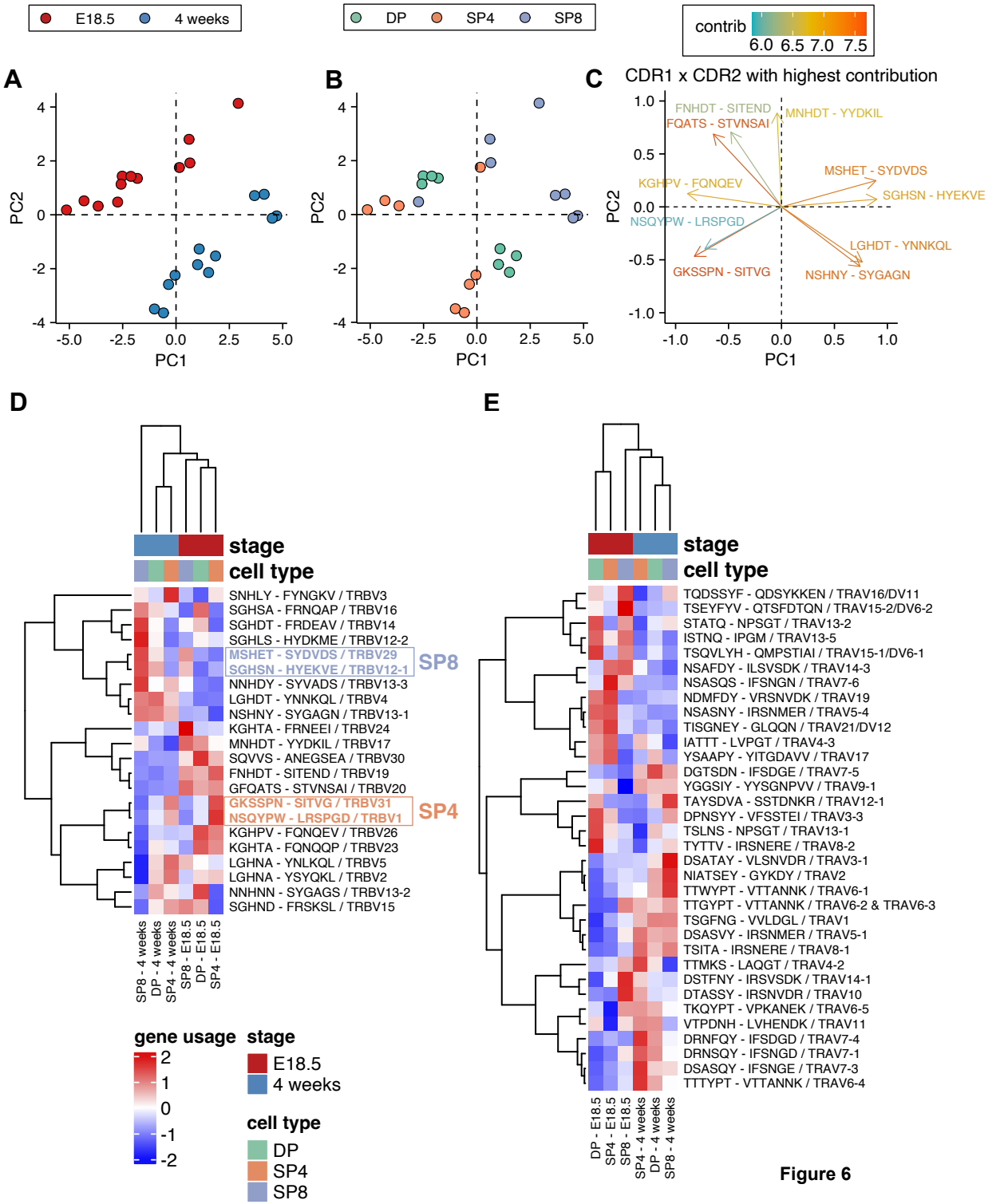
E18.5
4 weeks
DP
SP4
SP8
contrib
6.0 6.5 7.0 7.5
A
B
C
CDR1 x CDR2 with highest contribution
PC1
PC2
FNHDT - SITEND
FQATS - STVNSAI
MNHDT - YYDKIL
MSHET - SYDVDS
KGHPV - FQNQEV
SGHSN - HYEKVE
NSQYPW - LRSPGD
LGHDT - YNNKQL
GKSSPN - SITVG
NSHNY - SYGAGN
D
stage
cell type
SNHLY - FYNGKV / TRBV3
SGHSA - FRNQAP / TRBV16
SGHDT - FRDEAV / TRBV14
SGHLS - HYDKME / TRBV12-2
MSHET - SYDVDS / TRBV29
SGHSN - HYEKVE / TRBV12-1
SP8
NNHDY - SYVADS / TRBV13-3
LGHDT - YNNKQL / TRBV4
NSHNY - SYGAGN / TRBV13-1
KGHTA - FRNEEI / TRBV24
MNHDT - YYDKIL / TRBV17
SQVVS - ANEGSEA / TRBV30
FNHDT - SITEND / TRBV19
GFQATS - STVNSAI / TRBV20
GKSSPN - SITVG / TRBV31
NSQYPW - LRSPGD / TRBV1
SP4
KGHPV - FQNQEV / TRBV26
KGHTA - FQNQQP / TRBV23
LGHNA - YNLKQL / TRBV5
LGHNA - YSYQKL / TRBV2
NNHNN - SYGAGS / TRBV13-2
SGHND - FRSKSL / TRBV15
SP8 - 4 weeks
DP - 4 weeks
SP4 - 4 weeks
SP8 - E18.5
DP - E18.5
SP4 - E18.5
gene usage
2
1
0
-1
-2
stage
E18.5
4 weeks
cell type
DP
SP4
SP8
E
stage
cell type
TQDSSYF - QDSYKKEN / TRAV16/DV11
TSEYFYV - QTSFDTQN / TRAV15-2/DV6-2
STATQ - NPSGT / TRAV13-2
ISTNQ - IPGM / TRAV13-5
TSQVLYH - QMPSTIAI / TRAV15-1/DV6-1
NSAFDY - ILSVSDK / TRAV14-3
NSASQS - IFSNGN / TRAV7-6
NDMFDY - VRSNVDK / TRAV19
NSASNY - IRSNMER / TRAV5-4
TISGNEY - GLQQN / TRAV21/DV12
IATTT - LVPGT / TRAV4-3
YSAAPY - YITGDAVV / TRAV17
DGTSDN - IFSDGE / TRAV7-5
YGGSIY - YYSGNPVV / TRAV9-1
TAYSDVA - SSTDNKR / TRAV12-1
DPNSYY - VFSSTEI / TRAV3-3
TSLNS - NPSGT / TRAV13-1
TYTTV - IRSNERE / TRAV8-2
DSATAY - VLSNVDR / TRAV3-1
NIATSEY - GYKDY / TRAV2
TTWYPT - VTTANNK / TRAV6-1
TTGYPT - VTTANNK / TRAV6-2 & TRAV6-3
TSGFNG - VVLDGL / TRAV1
DSASVY - IRSNMER / TRAV5-1
TSITA - IRSNERE / TRAV8-1
TTMKS - LAQGT / TRAV4-2
DSTFNY - IRSVSDK / TRAV14-1
DTASSY - IRSNVDR / TRAV10
TKQYPT - VPKANEK / TRAV6-5
VTPDNH - LVHENDK / TRAV11
DRNFQY - IFSDGD / TRAV7-4
DRNSQY - IFSNGD / TRAV7-1
DSASQY - IFSNGE / TRAV7-3
TTTYPT - VTTANNK / TRAV6-4
DP - E18.5
SP4 - E18.5
SP8 - E18.5
SP4 - 4 weeks
DP - 4 weeks
SP8 - 4 weeks

Figure 6

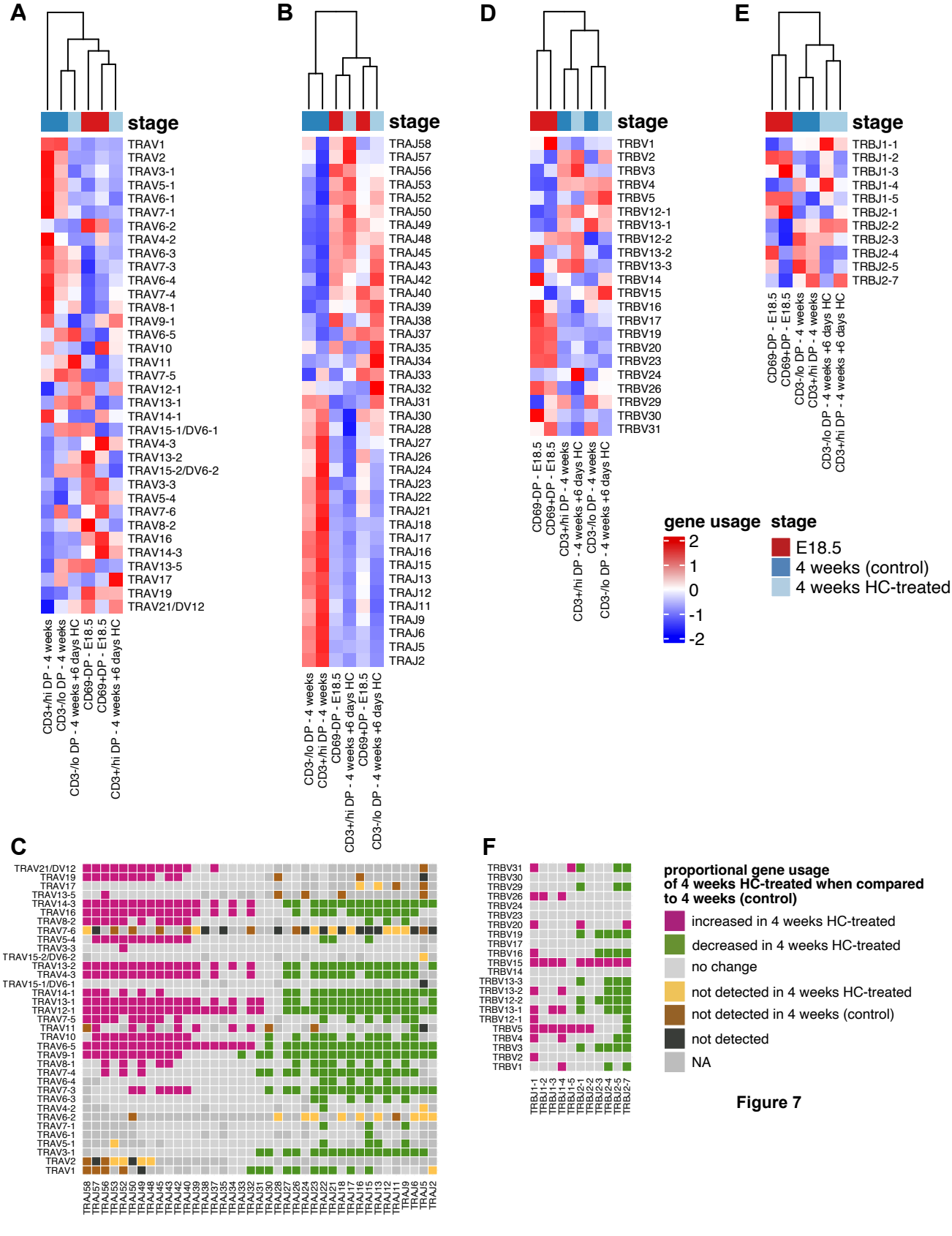
A
stage
TRAV1
TRAV2
TRAV3-1
TRAV5-1
TRAV6-1
TRAV7-1
TRAV6-2
TRAV4-2
TRAV6-3
TRAV7-3
TRAV6-4
TRAV7-4
TRAV8-1
TRAV9-1
TRAV6-5
TRAV10
TRAV11
TRAV7-5
TRAV12-1
TRAV13-1
TRAV14-1
TRAV15-1/DV6-1
TRAV4-3
TRAV13-2
TRAV15-2/DV6-2
TRAV3-3
TRAV5-4
TRAV7-6
TRAV8-2
TRAV16
TRAV14-3
TRAV13-5
TRAV17
TRAV19
TRAV21/DV12
CD3+/hi DP - 4 weeks
CD3-/lo DP - 4 weeks
CD3-/lo DP - 4 weeks +6 days HC
CD69-DP - E18.5
CD69+DP - E18.5
CD3+/hi DP - 4 weeks +6 days HC
B
stage
TRAJ58
TRAJ57
TRAJ56
TRAJ53
TRAJ52
TRAJ50
TRAJ49
TRAJ48
TRAJ45
TRAJ43
TRAJ42
TRAJ40
TRAJ39
TRAJ38
TRAJ37
TRAJ35
TRAJ34
TRAJ33
TRAJ32
TRAJ31
TRAJ30
TRAJ28
TRAJ27
TRAJ26
TRAJ24
TRAJ23
TRAJ22
TRAJ21
TRAJ18
TRAJ17
TRAJ16
TRAJ15
TRAJ13
TRAJ12
TRAJ11
TRAJ9
TRAJ6
TRAJ5
TRAJ2
CD3-/lo DP - 4 weeks
CD3+/hi DP - 4 weeks
CD69-DP - E18.5
CD3+/hi DP - 4 weeks +6 days HC
CD69+DP - E18.5
CD3-/lo DP - 4 weeks +6 days HC
D
stage
TRBV1
TRBV2
TRBV3
TRBV4
TRBV5
TRBV12-1
TRBV13-1
TRBV12-2
TRBV13-2
TRBV13-3
TRBV14
TRBV15
TRBV16
TRBV17
TRBV19
TRBV20
TRBV23
TRBV24
TRBV26
TRBV29
TRBV30
TRBV31
CD69-DP - E18.5
CD69+DP - E18.5
CD3+/hi DP - 4 weeks
CD3+/hi DP - 4 weeks +6 days HC
CD3-/lo DP - 4 weeks
CD3-/lo DP - 4 weeks +6 days HC
E
stage
TRBJ1-1
TRBJ1-2
TRBJ1-3
TRBJ1-4
TRBJ1-5
TRBJ2-1
TRBJ2-2
TRBJ2-3
TRBJ2-4
TRBJ2-5
TRBJ2-7
CD69-DP - E18.5
CD69+DP - E18.5
CD3-/lo DP - 4 weeks
CD3+/hi DP - 4 weeks
CD3-/lo DP - 4 weeks +6 days HC
CD3+/hi DP - 4 weeks +6 days HC
gene usage
2
1
0
-1
-2
stage
E18.5
4 weeks (control)
4 weeks HC-treated
C
TRAV21/DV12
TRAV19
TRAV17
TRAV13-5
TRAV14-3
TRAV16
TRAV8-2
TRAV7-6
TRAV5-4
TRAV3-3
TRAV15-2/DV6-2
TRAV13-2
TRAV4-3
TRAV15-1/DV6-1
TRAV14-1
TRAV13-1
TRAV12-1
TRAV7-5
TRAV11
TRAV10
TRAV6-5
TRAV9-1
TRAV8-1
TRAV7-4
TRAV6-4
TRAV7-3
TRAV6-3
TRAV4-2
TRAV6-2
TRAV7-1
TRAV6-1
TRAV5-1
TRAV3-1
TRAV2
TRAV1
TRAJ58
TRAJ57
TRAJ56
TRAJ53
TRAJ52
TRAJ50
TRAJ49
TRAJ48
TRAJ45
TRAJ43
TRAJ42
TRAJ40
TRAJ39
TRAJ38
TRAJ37
TRAJ35
TRAJ34
TRAJ33
TRAJ32
TRAJ31
TRAJ30
TRAJ28
TRAJ27
TRAJ26
TRAJ24
TRAJ23
TRAJ22
TRAJ21
TRAJ18
TRAJ17
TRAJ16
TRAJ15
TRAJ13
TRAJ12
TRAJ11
TRAJ9
TRAJ6
TRAJ5
TRAJ2
F
TRBV31
TRBV30
TRBV29
TRBV26
TRBV24
TRBV23
TRBV20
TRBV19
TRBV17
TRBV16
TRBV15
TRBV14
TRBV13-3
TRBV13-2
TRBV12-2
TRBV13-1
TRBV12-1
TRBV5
TRBV4
TRBV3
TRBV2
TRBV1
TRBJ1-1
TRBJ1-2
TRBJ1-3
TRBJ1-4
TRBJ1-5
TRBJ2-1
TRBJ2-2
TRBJ2-3
TRBJ2-4
TRBJ2-5
TRBJ2-7
proportional gene usage
of 4 weeks HC-treated when compared
to 4 weeks (control)
increased in 4 weeks HC-treated
decreased in 4 weeks HC-treated
no change
not detected in 4 weeks HC-treated
not detected in 4 weeks (control)
not detected
NA

Figure 7

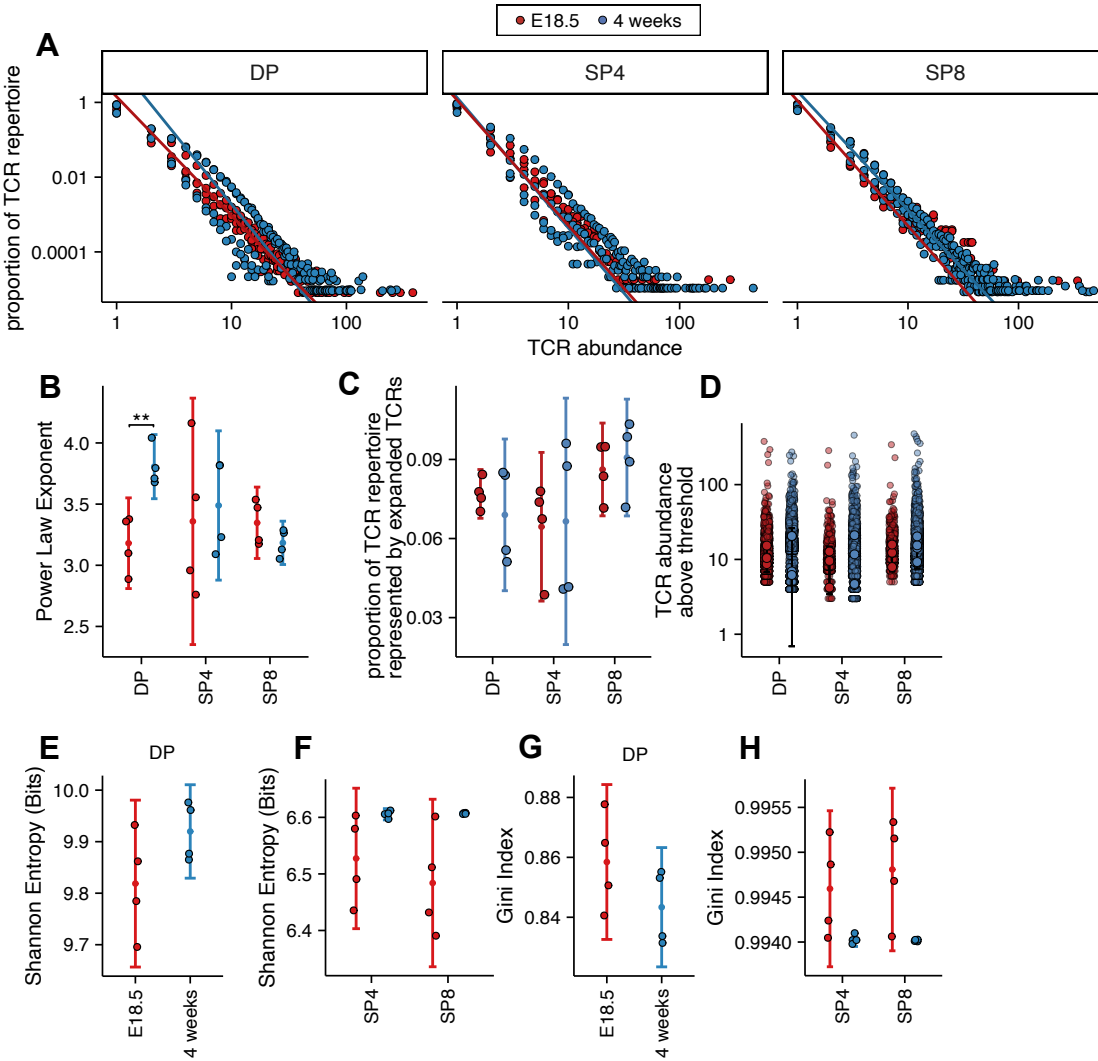

Supplementary Figure 1

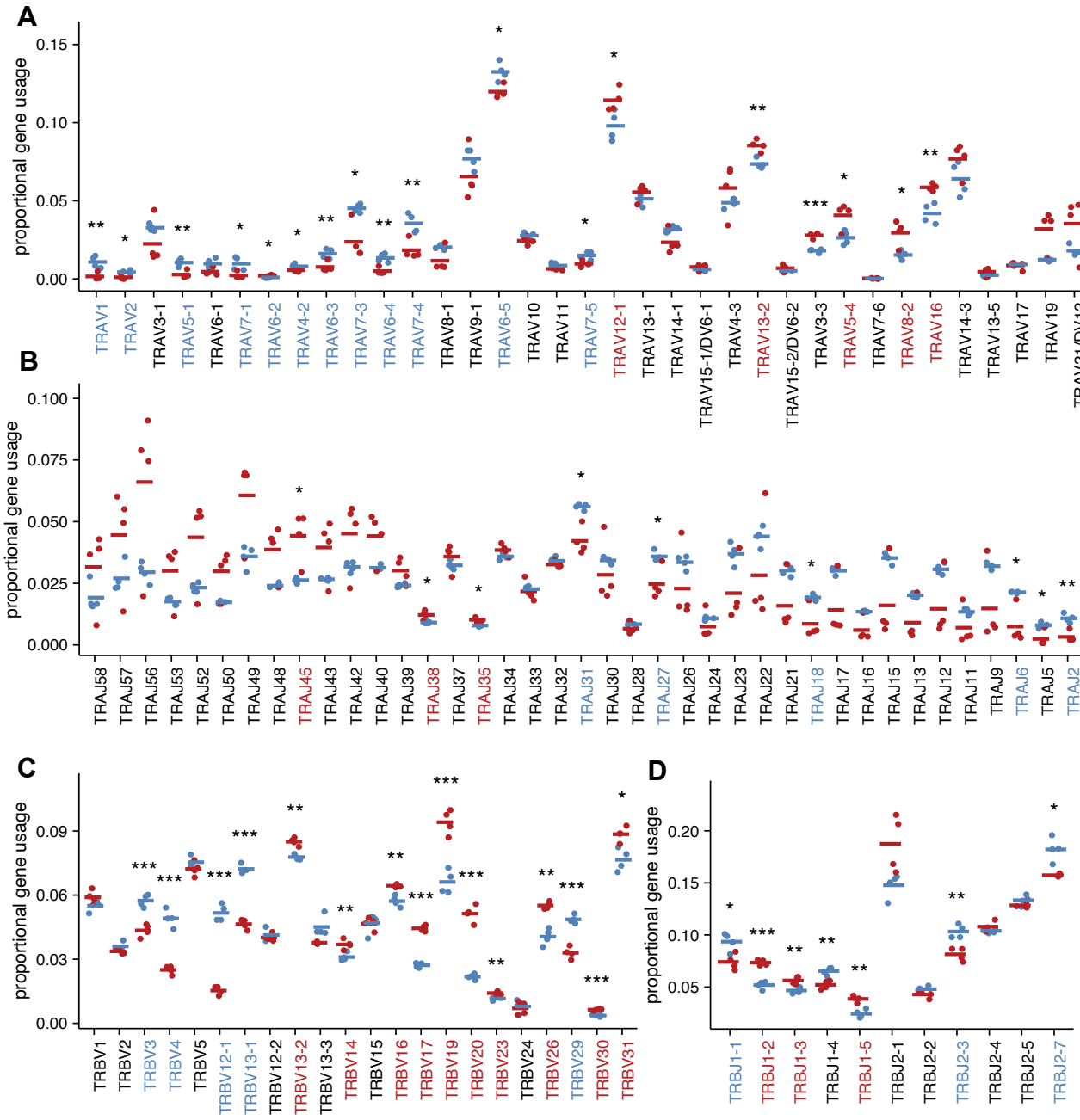

Supplementary Figure 2

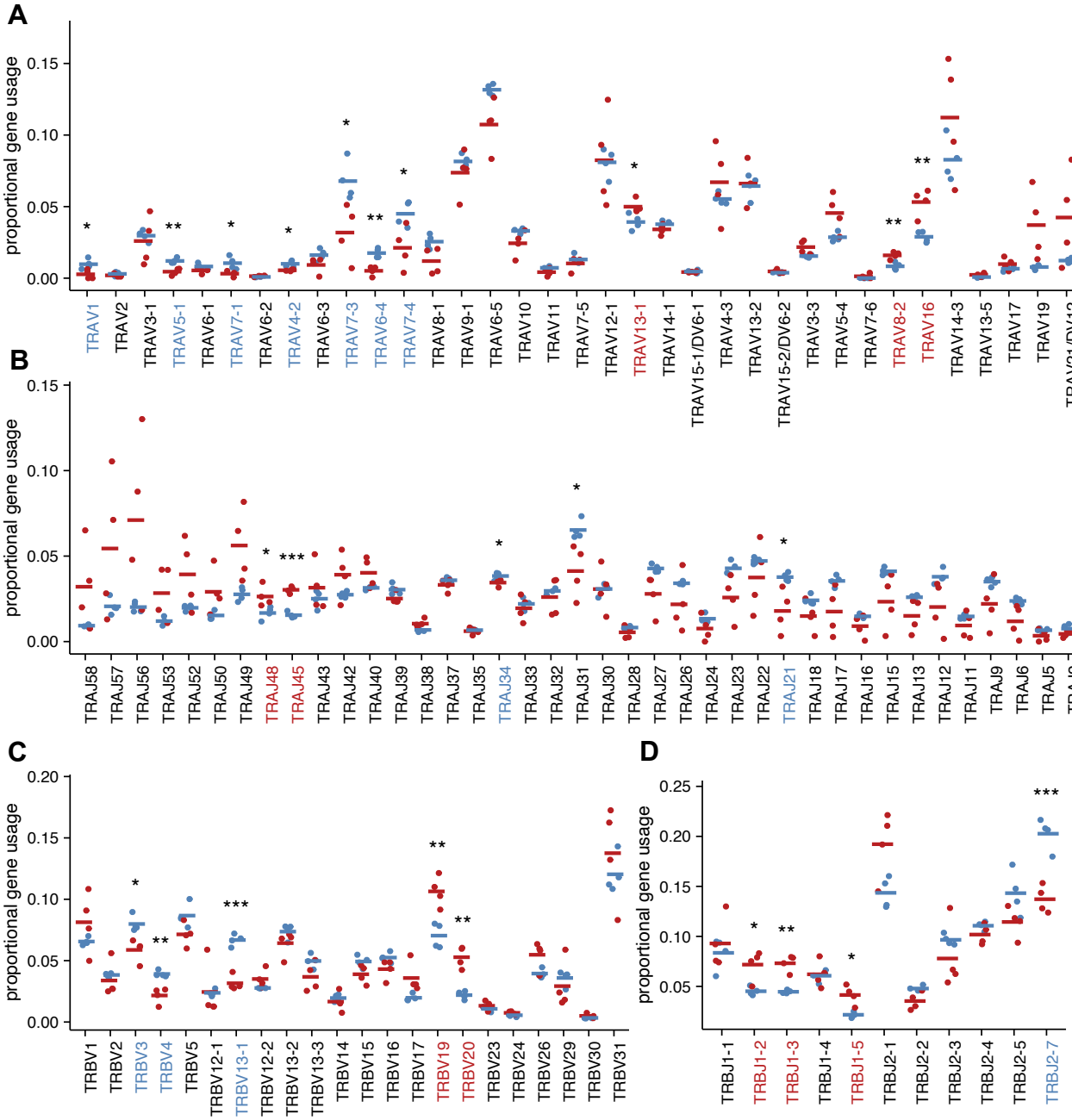

Supplementary Figure 3

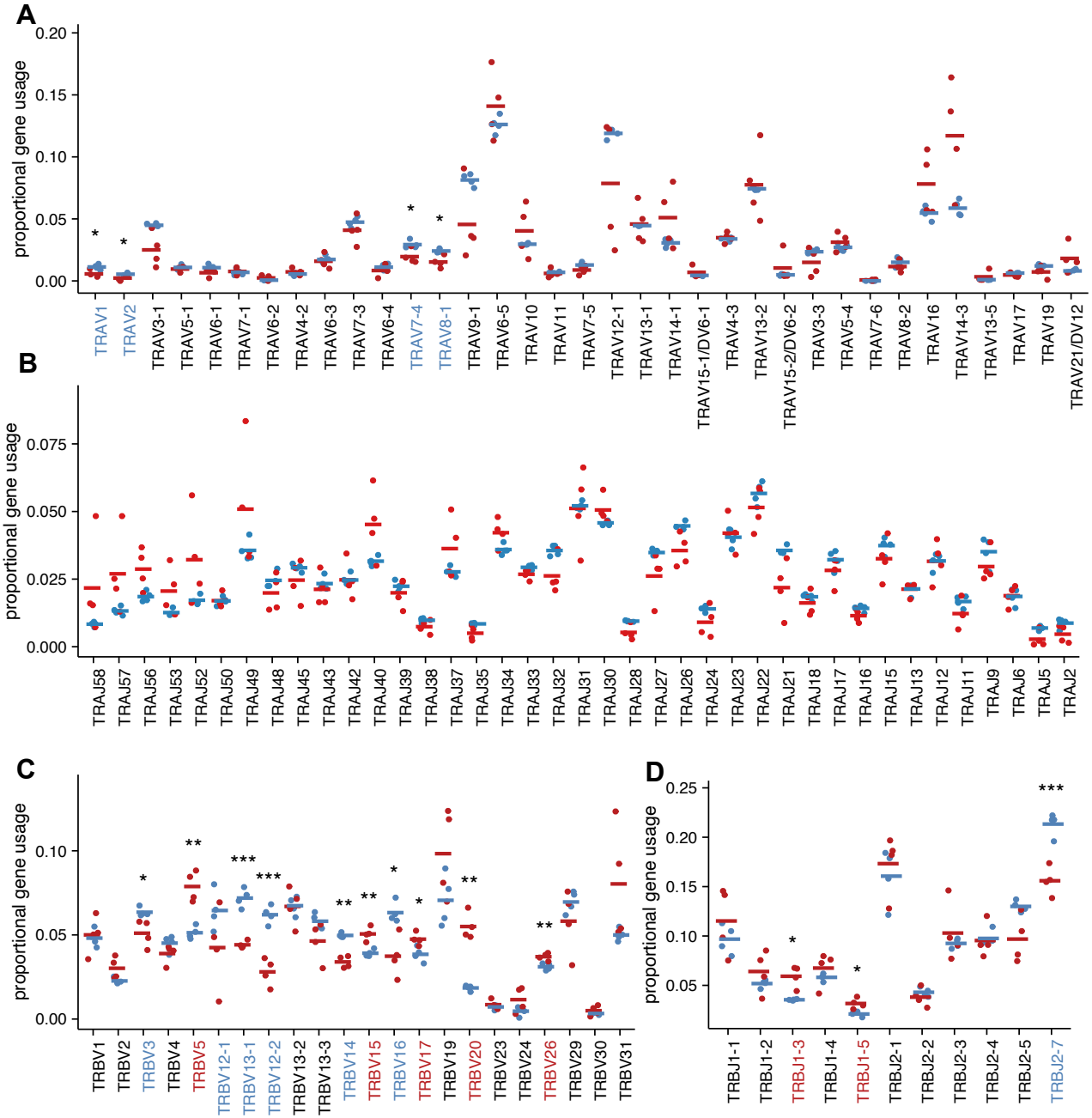

Supplementary Figure 4

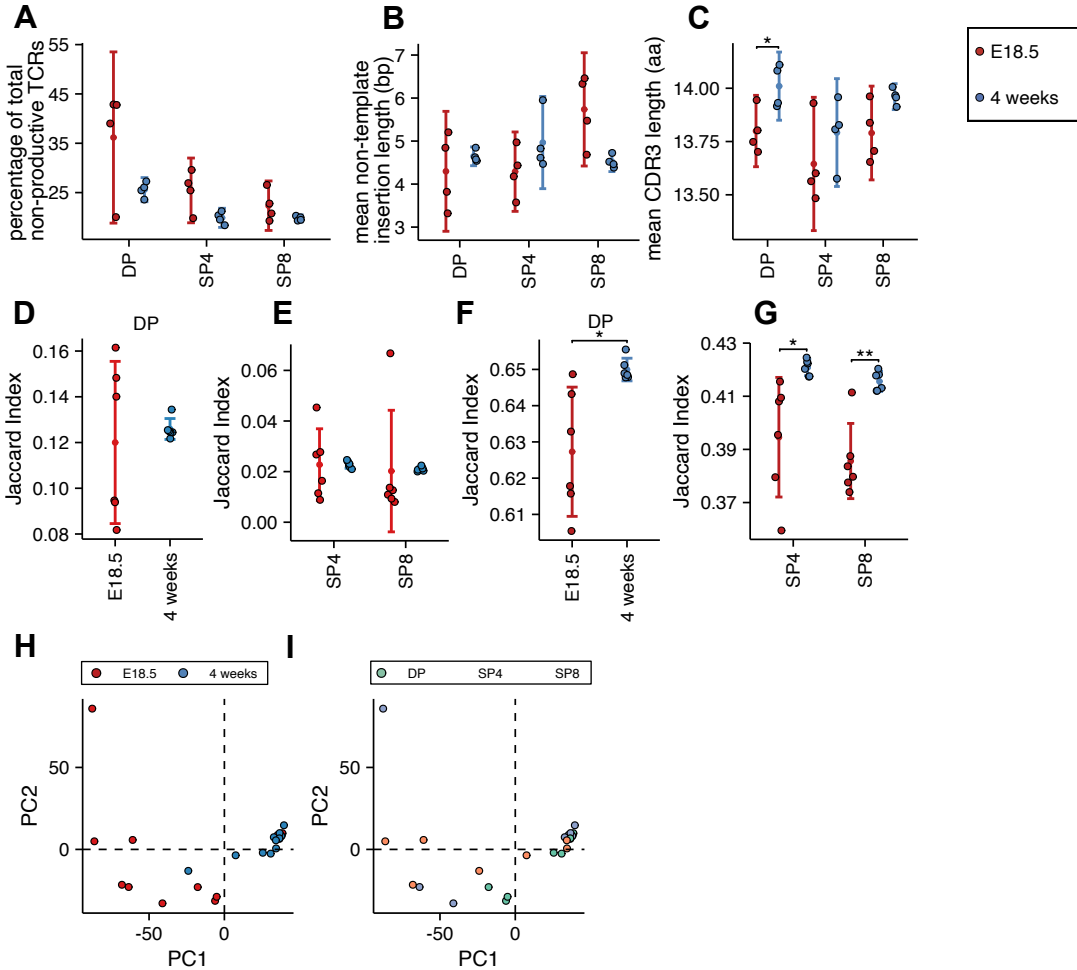

Supplementary Figure 5

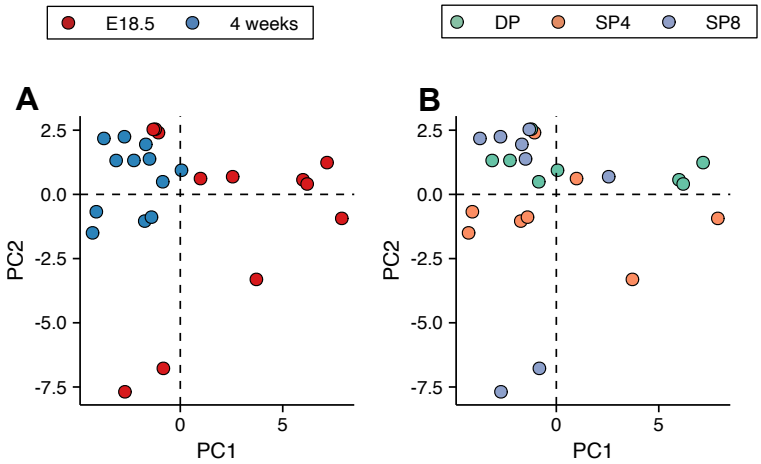

Supplementary Figure 6

Supplementary Tables

Supplementary Table 1 Antibody panel for staining thymus from 4 week mice.

Antibody	Clone	Supplier	Catalogue number
PE anti-mouse CD3	17AD	BioLegend	100206
PerCP/Cyanine5.5 anti-mouse CD4	RM4-4	BioLegend	116012
FITC anti-mouse CD8a	53-6.7	BioLegend	100706

Supplementary Table 2 Antibody panel for staining thymus from E18.5.

Antibody	Clone	Supplier	Catalogue number
Brilliant Violet 421 anti-mouse CD3	145-2C11	BioLegend	100335
APC anti-mouse CD4	RM4-4	BioLegend	116014
FITC anti-mouse CD8a	53-6.7	BioLegend	100706
PE anti-mouse CD69	H1.2F3	eBioscience	12-0691-83

Supplementary Table 3 | Primers used for TCR sequencing protocol

Name	Sequence	Description	Purification
TRAC3	GAGACCGAGGATCTTTTAACTGG	RT	desalted
TRBC2	GCTTTTGATGGCTCAAACAAGG	RT	desalted
6N_I8.1_6N_M13_2	[Phos]NNNNNNATCACGACNNNNNNCCAGGGTTTTCCCAGTCACGAC [SpcC3]	Ligation	HPLC
malphaRC1	CAGCAGGTTCTGGGTTCTGGATG	PCR1	desalted
mbetaRC1	GGGTGGAGTCACATTTCTCAGATCC	PCR1	desalted
SP2_M13	TTC AGA CGT GTG CTC TTC CGA TCT GTC GTG ACT GGG AAAA CCC TGG	PCR1	desalted
P5-SP1	AATGATACGGCGACCACCGAGATCTACACTCTTTCCCTACACGACGCTCTTCC	PCR2	desalted
mSP1-6N-I-6-aRC1	ACACTCTTTCCCTACACGACGCTCTTCCGATCTNNNNNNGCCAATCAGCAGGTTCTGGGTTCTGGATG	SP1	desalted
mSP1-6N-I-6-bRC1	ACACTCTTTCCCTACACGACGCTCTTCCGATCTNNNNNNGCCAATGGGTGGAGTCACATTTCTCAGATCC	SP1	desalted
mSP1-6N-I-7-aRC1	ACACTCTTTCCCTACACGACGCTCTTCCGATCTNNNNNNCAGATCCAGCAGGTTCTGGGTTCTGGATG	SP1	desalted
mSP1-6N-I-7-bRC1	ACACTCTTTCCCTACACGACGCTCTTCCGATCTNNNNNNCAGATCGGGTGGAGTCACATTTCTCAGATCC	SP1	desalted
mSP1-6N-I-8-aRC1	ACACTCTTTCCCTACACGACGCTCTTCCGATCTNNNNNNACTTGACAGCAGGTTCTGGGTTCTGGATG	SP1	desalted
mSP1-6N-I-8-bRC1	ACACTCTTTCCCTACACGACGCTCTTCCGATCTNNNNNNACTTGA GGGTGGAGTCACATTTCTCAGATCC	SP1	desalted
mSP1-6HN-I1-aRC1	ACACTCTTTCCCTACACGACGCTCTTCCGATCTHNHNNHATCACGCAGCAGGTTCTGGGTTCTGGATG	SP1	desalted
mSP1-6HN-I1-bRC1	ACACTCTTTCCCTACACGACGCTCTTCCGATCTHNHNNHATCACGGGGTGGAGTCACATTTCTCAGATCC	SP1	desalted
mSP1-6HN-I2-aRC1	ACACTCTTTCCCTACACGACGCTCTTCCGATCTHNHNNHCGATGTCAGCAGGTTCTGGGTTCTGGATG	SP1	desalted
mSP1-6HN-I2-bRC1	ACACTCTTTCCCTACACGACGCTCTTCCGATCTHNHNNHCGATGTGGGTGGAGTCACATTTCTCAGATCC	SP1	desalted
mSP1-6HN-I3-aRC1	ACACTCTTTCCCTACACGACGCTCTTCCGATCTHNHNNHTTAGGCCAGCAGGTTCTGGGTTCTGGATG	SP1	desalted
mSP1-6HN-I3-bRC1	ACACTCTTTCCCTACACGACGCTCTTCCGATCTHNHNNHTTAGGCGGGTGGAGTCACATTTCTCAGATCC	SP1	desalted
mSP1-6HN-I4-aRC1	ACACTCTTTCCCTACACGACGCTCTTCCGATCTHNHNNHTGACCACAGCAGGTTCTGGGTTCTGGATG	SP1	desalted
mSP1-6HN-I4-bRC1	ACACTCTTTCCCTACACGACGCTCTTCCGATCTHNHNNHTGACCAGGGTGGAGTCACATTTCTCAGATCC	SP1	desalted
mSP1-6HN-I5-aRC1	ACACTCTTTCCCTACACGACGCTCTTCCGATCTHNHNNHACAGTGCAGCAGGTTCTGGGTTCTGGATG	SP1	desalted
mSP1-6HN-I5-bRC1	ACACTCTTTCCCTACACGACGCTCTTCCGATCTHNHNNHACAGTGGGGTGGAGTCACATTTCTCAGATCC	SP1	desalted
mSP1-6HN-I6-aRC1	ACACTCTTTCCCTACACGACGCTCTTCCGATCTHNHNNHGCCAATCAGCAGGTTCTGGGTTCTGGATG	SP1	desalted

mSP1-6HN-I6-bRC1	ACACTCTTTCCCTACACGACGCTCTTCCGATCTHNHNNHGCCAATGGGTGGAGTCACATTTCTCAGATCC	SP1	desalted
mSP1-6HN-I7-aRC1	ACACTCTTTCCCTACACGACGCTCTTCCGATCTHNHNNHCAGATCCAGCAGGTTCTGGGTTCTGGATG	SP1	desalted
mSP1-6HN-I7-bRC1	ACACTCTTTCCCTACACGACGCTCTTCCGATCTHNHNNHCAGATCGGGTGGAGTCACATTTCTCAGATCC	SP1	desalted
mSP1-6HN-I8-aRC1	ACACTCTTTCCCTACACGACGCTCTTCCGATCTHNHNNHACTTGACAGCAGGTTCTGGGTTCTGGATG	SP1	desalted
mSP1-6HN-I8-bRC1	ACACTCTTTCCCTACACGACGCTCTTCCGATCTHNHNNHACTTGAGGGTGGAGTCACATTTCTCAGATCC	SP1	desalted
mSP1-6HN-I9-aRC1	ACACTCTTTCCCTACACGACGCTCTTCCGATCTHNHNNHGATCAGCAGCAGGTTCTGGGTTCTGGATG	SP1	desalted
mSP1-6HN-I9-bRC1	ACACTCTTTCCCTACACGACGCTCTTCCGATCTHNHNNHGATCAGGGGTGGAGTCACATTTCTCAGATCC	SP1	desalted
mSP1-6HN-I10-aRC1	ACACTCTTTCCCTACACGACGCTCTTCCGATCTHNHNNHTAGCTTCAGCAGGTTCTGGGTTCTGGATG	SP1	desalted
mSP1-6HN-I10-bRC1	ACACTCTTTCCCTACACGACGCTCTTCCGATCTHNHNNHTAGCTTGGGTGGAGTCACATTTCTCAGATCC	SP1	desalted
mSP1-6HN-I11-aRC1	ACACTCTTTCCCTACACGACGCTCTTCCGATCTHNHNNHGGCTACCAGCAGGTTCTGGGTTCTGGATG	SP1	desalted
mSP1-6HN-I11-bRC1	ACACTCTTTCCCTACACGACGCTCTTCCGATCTHNHNNHGGCTACGGGTGGAGTCACATTTCTCAGATCC	SP1	desalted
mSP1-6HN-I12-aRC1	ACACTCTTTCCCTACACGACGCTCTTCCGATCTHNHNNHCTTGTACAGCAGGTTCTGGGTTCTGGATG	SP1	desalted
mSP1-6HN-I12-bRC1	ACACTCTTTCCCTACACGACGCTCTTCCGATCTHNHNNHCTTGTAGGGTGGAGTCACATTTCTCAGATCC	SP1	desalted
mSP1-6HN-I13-aRC1	ACACTCTTTCCCTACACGACGCTCTTCCGATCTHNHNNHTAGACTCAGCAGGTTCTGGGTTCTGGATG	SP1	desalted
mSP1-6HN-I13-bRC1	ACACTCTTTCCCTACACGACGCTCTTCCGATCTHNHNNHTAGACTGGGTGGAGTCACATTTCTCAGATCC	SP1	desalted
P7-I8.15_SP2	CAAGCAGAAGACGGCATACGAGATCTACCAGGGTGACTGGAGTTCAGACGTGTGCTCTTCCGATC	SP2 P7	desalted
P7-I8.16_SP2	CAAGCAGAAGACGGCATACGAGATCATGCTTAGTGACTGGAGTTCAGACGTGTGCTCTTCCGATC	SP2 P7	desalted
P7-I8.17_SP2	CAAGCAGAAGACGGCATACGAGATGCACATCTGTGACTGGAGTTCAGACGTGTGCTCTTCCGATC	SP2 P7	desalted
P7-I8.18_SP2	CAAGCAGAAGACGGCATACGAGATTGCTCGACGTGACTGGAGTTCAGACGTGTGCTCTTCCGATC	SP2 P7	desalted
P7-I8.19_SP2	CAAGCAGAAGACGGCATACGAGATAGCAATTCGTGACTGGAGTTCAGACGTGTGCTCTTCCGATC	SP2 P7	desalted
P7-I8.20_SP2	CAAGCAGAAGACGGCATACGAGATAGTTGCTTGTGACTGGAGTTCAGACGTGTGCTCTTCCGATC	SP2 P7	desalted
P7-I8.21_SP2	CAAGCAGAAGACGGCATACGAGATCCAGTTAGGTGACTGGAGTTCAGACGTGTGCTCTTCCGATC	SP2 P7	desalted
P7-I8.22_SP2	CAAGCAGAAGACGGCATACGAGATTTGAGCCTGTGACTGGAGTTCAGACGTGTGCTCTTCCGATC	SP2 P7	desalted
P7-I8.23_SP2	CAAGCAGAAGACGGCATACGAGATACCAACTGGTGACTGGAGTTCAGACGTGTGCTCTTCCGATC	SP2 P7	desalted
P7-I8.24_SP2	CAAGCAGAAGACGGCATACGAGATGGTCCAGAGTGACTGGAGTTCAGACGTGTGCTCTTCCGATC	SP2 P7	desalted

P7-I8.25_SP2	CAAGCAGAAGACGGCATACGAGATGTATAACAGTGACTGGAGTTCAGACGTGTGCTCTTCCGATC	SP2 P7	desalted
P7-I8.26_SP2	CAAGCAGAAGACGGCATACGAGATTTCGCTGAGTGACTGGAGTTCAGACGTGTGCTCTTCCGATC	SP2 P7	desalted
P7_L27	CAAGCAGAAGACGGCATACGAGAT CGCTATGT GTGACTGGAGTTCAGACGTGTGCTCTTCCGATC	SP2 P7	desalted
P7_L28	CAAGCAGAAGACGGCATACGAGAT TAAGCACA GTGACTGGAGTTCAGACGTGTGCTCTTCCGATC	SP2 P7	desalted
P7_L29	CAAGCAGAAGACGGCATACGAGAT GTAACATC GTGACTGGAGTTCAGACGTGTGCTCTTCCGATC	SP2 P7	desalted
P7_L30	CAAGCAGAAGACGGCATACGAGAT ACTAAGAC GTGACTGGAGTTCAGACGTGTGCTCTTCCGATC	SP2 P7	desalted
P7_L31	CAAGCAGAAGACGGCATACGAGAT TGTAACTC GTGACTGGAGTTCAGACGTGTGCTCTTCCGATC	SP2 P7	desalted
P7_L32	CAAGCAGAAGACGGCATACGAGAT AACAATGG GTGACTGGAGTTCAGACGTGTGCTCTTCCGATC	SP2 P7	desalted
P7_L33	CAAGCAGAAGACGGCATACGAGAT CCTTCGCA GTGACTGGAGTTCAGACGTGTGCTCTTCCGATC	SP2 P7	desalted
P7_L34	CAAGCAGAAGACGGCATACGAGAT GACCGTTG GTGACTGGAGTTCAGACGTGTGCTCTTCCGATC	SP2 P7	desalted
P7_L35	CAAGCAGAAGACGGCATACGAGAT TCTGCAAG GTGACTGGAGTTCAGACGTGTGCTCTTCCGATC	SP2 P7	desalted
P7_L36	CAAGCAGAAGACGGCATACGAGAT CACATCCT GTGACTGGAGTTCAGACGTGTGCTCTTCCGATC	SP2 P7	desalted
P7_L37	CAAGCAGAAGACGGCATACGAGAT AGGATCTA GTGACTGGAGTTCAGACGTGTGCTCTTCCGATC	SP2 P7	desalted
P7_L38	CAAGCAGAAGACGGCATACGAGAT GTCATCTA GTGACTGGAGTTCAGACGTGTGCTCTTCCGATC	SP2 P7	desalted
P7_L39	CAAGCAGAAGACGGCATACGAGAT GAACCTAG GTGACTGGAGTTCAGACGTGTGCTCTTCCGATC	SP2 P7	desalted
P7_L40	CAAGCAGAAGACGGCATACGAGAT TTACGCAC GTGACTGGAGTTCAGACGTGTGCTCTTCCGATC	SP2 P7	desalted
P7_L41	CAAGCAGAAGACGGCATACGAGAT AGGTGCGA GTGACTGGAGTTCAGACGTGTGCTCTTCCGATC	SP2 P7	desalted
P7_L42	CAAGCAGAAGACGGCATACGAGAT CATGATCG GTGACTGGAGTTCAGACGTGTGCTCTTCCGATC	SP2 P7	desalted
P7_L43	CAAGCAGAAGACGGCATACGAGAT GCCGCAAC GTGACTGGAGTTCAGACGTGTGCTCTTCCGATC	SP2 P7	desalted
P7_L44	CAAGCAGAAGACGGCATACGAGAT TTATATCT GTGACTGGAGTTCAGACGTGTGCTCTTCCGATC	SP2 P7	desalted
P7_L45	CAAGCAGAAGACGGCATACGAGAT CTGTGGCG GTGACTGGAGTTCAGACGTGTGCTCTTCCGATC	SP2 P7	desalted
P7_L46	CAAGCAGAAGACGGCATACGAGAT AACGCATT GTGACTGGAGTTCAGACGTGTGCTCTTCCGATC	SP2 P7	desalted
P7_L47	CAAGCAGAAGACGGCATACGAGAT AACTTGAC GTGACTGGAGTTCAGACGTGTGCTCTTCCGATC	SP2 P7	desalted
P7_L48	CAAGCAGAAGACGGCATACGAGAT CGCCTTCC GTGACTGGAGTTCAGACGTGTGCTCTTCCGATC	SP2 P7	desalted
P7_L49	CAAGCAGAAGACGGCATACGAGAT GACCAGGA GTGACTGGAGTTCAGACGTGTGCTCTTCCGATC	SP2 P7	desalted

P7_L50	CAAGCAGAAGACGGCATACGAGAT TCCTTGGT GTGACTGGAGTTCAGACGTGTGCTCTTCCGATC	SP2 P7	desalted
P7_L51	CAAGCAGAAGACGGCATACGAGAT AAGACACT GTGACTGGAGTTCAGACGTGTGCTCTTCCGATC	SP2 P7	desalted
P7_L52	CAAGCAGAAGACGGCATACGAGAT CTGTAATC GTGACTGGAGTTCAGACGTGTGCTCTTCCGATC	SP2 P7	desalted
P7_L53	CAAGCAGAAGACGGCATACGAGAT GAAGAAGT GTGACTGGAGTTCAGACGTGTGCTCTTCCGATC	SP2 P7	desalted
P7_L54	CAAGCAGAAGACGGCATACGAGAT TAATGAAC GTGACTGGAGTTCAGACGTGTGCTCTTCCGATC	SP2 P7	desalted
P7_L55	CAAGCAGAAGACGGCATACGAGAT TCCAGCAA GTGACTGGAGTTCAGACGTGTGCTCTTCCGATC	SP2 P7	desalted
P7_L56	CAAGCAGAAGACGGCATACGAGAT GTCCACAG GTGACTGGAGTTCAGACGTGTGCTCTTCCGATC	SP2 P7	desalted
P7_L57	CAAGCAGAAGACGGCATACGAGAT CAATAGTC GTGACTGGAGTTCAGACGTGTGCTCTTCCGATC	SP2 P7	desalted
P7_L58	CAAGCAGAAGACGGCATACGAGAT AGGTAAGG GTGACTGGAGTTCAGACGTGTGCTCTTCCGATC	SP2 P7	desalted
P7_L59	CAAGCAGAAGACGGCATACGAGAT TACTTAGC GTGACTGGAGTTCAGACGTGTGCTCTTCCGATC	SP2 P7	desalted
P7_L60	CAAGCAGAAGACGGCATACGAGAT GAAGGAAG GTGACTGGAGTTCAGACGTGTGCTCTTCCGATC	SP2 P7	desalted
P7_L61	CAAGCAGAAGACGGCATACGAGAT CATAGCGA GTGACTGGAGTTCAGACGTGTGCTCTTCCGATC	SP2 P7	desalted
P7_L62	CAAGCAGAAGACGGCATACGAGAT ATTGTCTG GTGACTGGAGTTCAGACGTGTGCTCTTCCGATC	SP2 P7	desalted
P7_L63	CAAGCAGAAGACGGCATACGAGAT CAACTCTC GTGACTGGAGTTCAGACGTGTGCTCTTCCGATC	SP2 P7	desalted
P7_L64	CAAGCAGAAGACGGCATACGAGAT ATTCTAGG GTGACTGGAGTTCAGACGTGTGCTCTTCCGATC	SP2 P7	desalted
P7_L65	CAAGCAGAAGACGGCATACGAGAT TGCTGCTG GTGACTGGAGTTCAGACGTGTGCTCTTCCGATC	SP2 P7	desalted
P7_L66	CAAGCAGAAGACGGCATACGAGAT GCCTAGCC GTGACTGGAGTTCAGACGTGTGCTCTTCCGATC	SP2 P7	desalted
P7_L67	CAAGCAGAAGACGGCATACGAGAT CCTATGCC GTGACTGGAGTTCAGACGTGTGCTCTTCCGATC	SP2 P7	desalted
P7_L68	CAAGCAGAAGACGGCATACGAGAT ATAGCGTC GTGACTGGAGTTCAGACGTGTGCTCTTCCGATC	SP2 P7	desalted
P7_L69	CAAGCAGAAGACGGCATACGAGAT TGTCGGAT GTGACTGGAGTTCAGACGTGTGCTCTTCCGATC	SP2 P7	desalted
P7_L70	CAAGCAGAAGACGGCATACGAGAT GACAGTAA GTGACTGGAGTTCAGACGTGTGCTCTTCCGATC	SP2 P7	desalted
P7_L71	CAAGCAGAAGACGGCATACGAGAT GCCGTCGA GTGACTGGAGTTCAGACGTGTGCTCTTCCGATC	SP2 P7	desalted
P7_L72	CAAGCAGAAGACGGCATACGAGAT TATCCAGG GTGACTGGAGTTCAGACGTGTGCTCTTCCGATC	SP2 P7	desalted
P7_L73	CAAGCAGAAGACGGCATACGAGAT ATTATGTT GTGACTGGAGTTCAGACGTGTGCTCTTCCGATC	SP2 P7	desalted
P7_L74	CAAGCAGAAGACGGCATACGAGAT CCAACATT GTGACTGGAGTTCAGACGTGTGCTCTTCCGATC	SP2 P7	desalted

P7_L75	CAAGCAGAAGACGGCATACGAGAT GATATCCA GTGACTGGAGTTCAGACGTGTGCTCTTCCGATC	SP2 P7	desalted
P7_L76	CAAGCAGAAGACGGCATACGAGAT TGCAAGTA GTGACTGGAGTTCAGACGTGTGCTCTTCCGATC	SP2 P7	desalted
P7_L77	CAAGCAGAAGACGGCATACGAGAT AATGTTCT GTGACTGGAGTTCAGACGTGTGCTCTTCCGATC	SP2 P7	desalted
P7_L78	CAAGCAGAAGACGGCATACGAGAT CAGCGGTA GTGACTGGAGTTCAGACGTGTGCTCTTCCGATC	SP2 P7	desalted
P7_L79	CAAGCAGAAGACGGCATACGAGAT ATTCCTCT GTGACTGGAGTTCAGACGTGTGCTCTTCCGATC	SP2 P7	desalted
P7_L80	CAAGCAGAAGACGGCATACGAGAT CTGCGGAT GTGACTGGAGTTCAGACGTGTGCTCTTCCGATC	SP2 P7	desalted
P7_L81	CAAGCAGAAGACGGCATACGAGAT GTCTGATG GTGACTGGAGTTCAGACGTGTGCTCTTCCGATC	SP2 P7	desalted
P7_L82	CAAGCAGAAGACGGCATACGAGAT TATCTGCC GTGACTGGAGTTCAGACGTGTGCTCTTCCGATC	SP2 P7	desalted
P7_L83	CAAGCAGAAGACGGCATACGAGAT ACACGATC GTGACTGGAGTTCAGACGTGTGCTCTTCCGATC	SP2 P7	desalted
P7_L84	CAAGCAGAAGACGGCATACGAGAT CCAGAGCT GTGACTGGAGTTCAGACGTGTGCTCTTCCGATC	SP2 P7	desalted
P7_L85	CAAGCAGAAGACGGCATACGAGAT GACCTAAC GTGACTGGAGTTCAGACGTGTGCTCTTCCGATC	SP2 P7	desalted
P7_L86	CAAGCAGAAGACGGCATACGAGAT TCGCCTTG GTGACTGGAGTTCAGACGTGTGCTCTTCCGATC	SP2 P7	desalted
P7_L87	CAAGCAGAAGACGGCATACGAGAT CCTACCAT GTGACTGGAGTTCAGACGTGTGCTCTTCCGATC	SP2 P7	desalted
P7_L88	CAAGCAGAAGACGGCATACGAGAT TCGCTAGA GTGACTGGAGTTCAGACGTGTGCTCTTCCGATC	SP2 P7	desalted
P7_L89	CAAGCAGAAGACGGCATACGAGAT AAGGATGT GTGACTGGAGTTCAGACGTGTGCTCTTCCGATC	SP2 P7	desalted
P7_L90	CAAGCAGAAGACGGCATACGAGAT CTAACTCG GTGACTGGAGTTCAGACGTGTGCTCTTCCGATC	SP2 P7	desalted
P7_L91	CAAGCAGAAGACGGCATACGAGAT ACAGGTAT GTGACTGGAGTTCAGACGTGTGCTCTTCCGATC	SP2 P7	desalted
P7_L92	CAAGCAGAAGACGGCATACGAGAT TCTCGGTC GTGACTGGAGTTCAGACGTGTGCTCTTCCGATC	SP2 P7	desalted
P7_L93	CAAGCAGAAGACGGCATACGAGAT ACAGTTGA GTGACTGGAGTTCAGACGTGTGCTCTTCCGATC	SP2 P7	desalted
P7_L94	CAAGCAGAAGACGGCATACGAGAT CTATGCGT GTGACTGGAGTTCAGACGTGTGCTCTTCCGATC	SP2 P7	desalted
P7_L95	CAAGCAGAAGACGGCATACGAGAT CAGGAGCC GTGACTGGAGTTCAGACGTGTGCTCTTCCGATC	SP2 P7	desalted
P7_L96	CAAGCAGAAGACGGCATACGAGAT AGGTCGCA GTGACTGGAGTTCAGACGTGTGCTCTTCCGATC	SP2 P7	desalted
P7_L97	CAAGCAGAAGACGGCATACGAGAT CAGCAAGG GTGACTGGAGTTCAGACGTGTGCTCTTCCGATC	SP2 P7	desalted
P7_L98	CAAGCAGAAGACGGCATACGAGAT ATTATCAA GTGACTGGAGTTCAGACGTGTGCTCTTCCGATC	SP2 P7	desalted
P7_L99	CAAGCAGAAGACGGCATACGAGAT TTAATCAG GTGACTGGAGTTCAGACGTGTGCTCTTCCGATC	SP2 P7	desalted

P7_L100	CAAGCAGAAGACGGCATACGAGAT CGTTACCA GTGACTGGAGTTCAGACGTGTGCTCTTCCGATC	SP2 P7	desalted
P7_L101	CAAGCAGAAGACGGCATACGAGAT AAGTAGAG GTGACTGGAGTTCAGACGTGTGCTCTTCCGATC	SP2 P7	desalted
P7_L102	CAAGCAGAAGACGGCATACGAGAT TTGAATAG GTGACTGGAGTTCAGACGTGTGCTCTTCCGATC	SP2 P7	desalted
P5	AATGATACGGCGACCACCGAGATCTACACT	QPCR	desalted
P7	CAAGCAGAAGACGGCATACGAGAT	QPCR	desalted

Supplementary Table 4 | Reagents and consumables for TCR sequencing protocol

Reagent	Supplier	Cat. No.
RQ1 RNase-Free DNase	Promega	M6101
RQ1 DNase 10X Reaction Buffer	Promega	M6101
RQ1 Dnase Stop Solution	Promega	M6101
RNase free water	Invitrogen	10977-035
dNTPs (10 mM)	Promega	U1515
SuperScript III RT (200 U/µl)	Invitrogen	18080085
5X First-Strand (FS) Buffer	Invitrogen	18080085
0.1 M DTT	Invitrogen	18080085
RNasin	Promega	N2115
Minelute PCR Purification kit	Qiagen	28006
T4 RNA Ligase Reaction Buffer	NEB	M0204L
Adenosine-5'-Triphosphate (ATP)	NEB	M0204L
PEG 8000	NEB	M0204L
T4 RNA Ligase 1 (ssRNA Ligase)	NEB	M0204L
BSA (20 mg/mL)	NEB	B9000S
Hexammine cobalt(III) chloride (HCC)	Sigma	H7891-5G
Agencourt AMPure beads XP	Beckman Coulter	A63881
5x Phusion HF buffer	NEB	M0530L
Phusion Polymerase	NEB	M0530L
ROX Reference Dye	Invitrogen	12223012
SYBR Green I Nucleic Acid Gel Stain 10,000×	Invitrogen	S7563
DMSO for molecular biology	Sigma	D8418-50ML
Qubit dsDNA HS Assay Kit	ThermoFisher Scientific	Q32854
Qubit Assay Tubes	ThermoFisher Scientific	Q32856
High Sensitivity D1000 ScreenTape	Agilent	5067-5584
High Sensitivity D1000 Reagents	Agilent	5067-5585
High Sensitivity D1000 Ladder	Agilent	5067-5587
96-well Plates	Agilent	5042-8502
96-well Plate Foil Seal	Agilent	5067-5154
Pippin Gel Cassette 1.5% agarose dye free 250bp-1.5kb	Sage Science	CDF1510
PhiX Control V3	Illumina	FC-110-3001
MiSeq Reagent Kit v2 (500-cycles)	Illumina	MS-102-2003
Eppendorf DNA LoBind Polypropylene Microcentrifuge Tube	FisherScientific	10051232
96-well PCR plate semi skirted	Starlab	I1402-9700C
Adhesive PCR Plate Seal	SLS	4ti-0500
PicoPure RNA Isolation Kit	Applied Biosystems	KIT0204
500/550 Mid Output Kit v2.5 (300 Cycles)	Illumina	20024905
Blitz Away RNase spray	Serem Biotech	40-1735-10
Tris (1M), pH 7.0, RNase-free	ThermoFisher Scientific	AM9850G

Sodium hydroxide solution for molecular biology, 10M in H2O	Sigma	72068-100ML